Public document

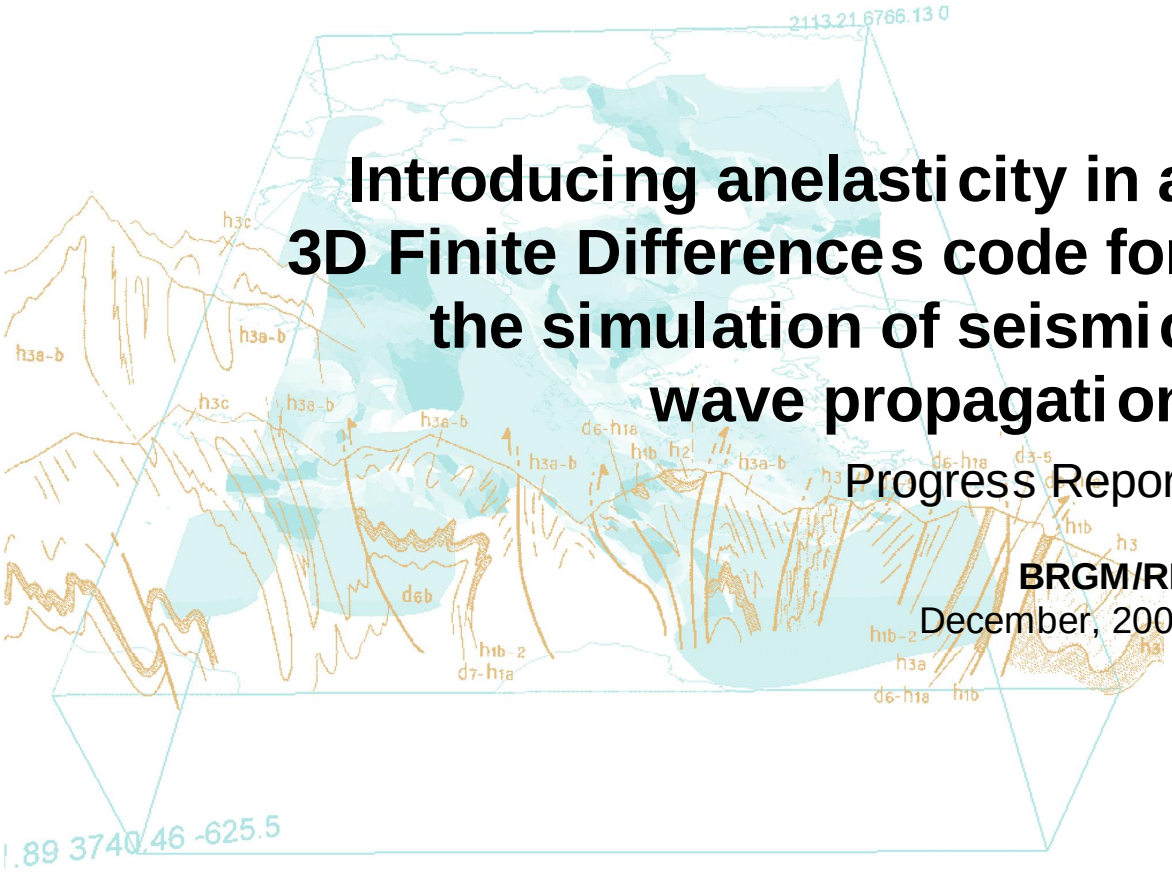

Introducing anelasticity in a 3D Finite Differences code for the simulation of seismic wave propagation

Progress Report

BRGM/RP

December, 2009

Geoscience for a sustainable Earth

brgm

Public document

Introducing anelasticity in a 3D Finite Differences code for the simulation of seismic wave propagation

Progress Report

BRGM/RP
December, 2009

Study carried out as part of
Research activities - BRGM 2009 ARN41 and STI04

Ducellier A., Aochi H., Lee-tin-yien Y.

Checked by:	**Approved by**:
Name: Florent De Martin	Name: Hormoz Modaressi
Date:	Date:
Signature:	Signature:

BRGM's quality management system is certified ISO 9001:2000 by AFAQ

Geoscience for a sustainable Earth
brgm

Keywords: Seismic wave propagation, Convolutional Perfectly Matched Layer, Finite Differences, Anelasticity.

In bibliography, this report should be cited as follows:

Ducellier A., Aochi H., Lee-tin-yien Y. (2009) ï Introducing anelasticity in a 3D Finite Differences code for the simulation of seismic wave propagation. Year 2009 ï BRGM / RP-55923-FR, 62 p.

Synopsis

The introduction of parallel computing has made possible the simulation of seismic wave propagation in elastic media with numerical methods like finite differences over large spatial domains compared to the wavelength. However, when a seismic pulse propagates along a large distance, dispersion due to material imperfections causes wave attenuation. Moreover, it is known that shallower crust layers sometimes attenuate significantly the radiating wave energy.

Taking account anelastic attenuation requires much more memory than numerical simulation in an elastic medium. Several methods were developed to approximate the anelastic quality factor over a specified frequency band while keeping the additional cost of memory relatively low.

The aim of this report is to explain the implementation in a 3D finite differences code of two anelastic methods proposed by Day and Bradley (2001) and Kristek and Moczo (2003) and to test and compare their efficiency.

Contents

List of illustrations

1. Introduction

The introduction of parallel computing has made possible the simulation of seismic wave propagation in elastic media with numerical methods like finite differences over large spatial domains compared to the wavelength. However, when a seismic pulse propagates along a large distance, dispersion due to material imperfections causes wave attenuation. Moreover, it is known that shallower crust layers sometimes attenuate significantly the radiating wave energy.

Taking account anelastic attenuation requires much more memory than numerical simulation in an elastic medium. Several methods were developed to approximate the anelastic quality factor over a specified frequency band while keeping the additional cost of memory relatively low.

The BRGM has developed a parallel 3D finite differences code for the simulation of seismic wave propagation in elastic media: ONDES3D. Within the framework of BRGM research activities and an internship during the year 2009 (Lee-tin-yien, 2009), two anelastic methods were implemented in ONDES3D: the method proposed by Day and Bradley (2001) and the method proposed by Kristek and Moczo (2003), which is supposed to be an improvement of the former. The aim of this report is to explain the implementation of these two anelastic methods and to test and compare their efficiency.

In the first chapter of this report, the theoretical aspects of the two anelastic methods are presented and, in the second chapter, several tests which were carried out to test the efficiency of the two methods and to compare them are exposed.

2. Anelasticity: theoretical aspects

ONDES3D is a 3D finite differences code developed by the BRGM for the simulation of seismic wave propagation. A first method to introduce attenuation was present in the elastic version of ONDES3D. At each time step, each component of velocity and stress were multiplied by the amplification factor given in Equation (1), where dt is the time step of the computation, Q is the anelastic quality factor and f_0 is a reference frequency.

$$a = \exp\left(-\frac{\pi f_0 dt}{Q}\right) \qquad (1)$$

However, this method is not very efficient to accurately model realistic anelastic attenuation. In order to solve this problem, more complex methods were developed in the literature to approximate the anelastic quality factor over a specified frequency band while keeping the additional cost of memory relatively low. Two of them are chosen to be implemented in ONDES3D. Their theoretical formulations are exposed hereafter.

2.1. METHOD OF DAY AND BRADLEY

The first anelastic method implemented in ONDES3D was proposed by Day (1998) and Day and Bradley (2001).

2.1.1. Theoretical formulation

In the elastic case, the differential form of the 3D elastic wave equation can be written in the Cartesian coordinates (x, y, z) in terms of velocity (v_x, v_y, v_z) and stress ($\mathring{u}_{xx}$, $\mathring{u}_{yy}$, $\mathring{u}_{zz}$, $\mathring{u}_{xy}$, $\mathring{u}_{xz}$, $\mathring{u}_{yz}$) as Equation (2), where ɟ is density and ə and ε are bulk and shear moduli, respectively.

$$\rho \frac{\partial v_x}{\partial t} = \frac{\partial \sigma_{xx}}{\partial x} + \frac{\partial \sigma_{xy}}{\partial y} + \frac{\partial \sigma_{xz}}{\partial z}$$

$$\rho \frac{\partial v_y}{\partial t} = \frac{\partial \sigma_{xy}}{\partial x} + \frac{\partial \sigma_{yy}}{\partial y} + \frac{\partial \sigma_{yz}}{\partial z}$$

$$\rho \frac{\partial v_z}{\partial t} = \frac{\partial \sigma_{xz}}{\partial x} + \frac{\partial \sigma_{yz}}{\partial y} + \frac{\partial \sigma_{zz}}{\partial z}$$

$$\frac{\partial \sigma_{xx}}{\partial t} = \left(\kappa - \frac{2\mu}{3}\right)\left(\frac{\partial v_x}{\partial x} + \frac{\partial v_y}{\partial y} + \frac{\partial v_z}{\partial z}\right) + 2\mu \frac{\partial v_x}{\partial x}$$

$$\frac{\partial \sigma_{yy}}{\partial t} = \left(\kappa - \frac{2\mu}{3}\right)\left(\frac{\partial v_x}{\partial x} + \frac{\partial v_y}{\partial y} + \frac{\partial v_z}{\partial z}\right) + 2\mu \frac{\partial v_y}{\partial y} \qquad \textbf{(2)}$$

$$\frac{\partial \sigma_{zz}}{\partial t} = \left(\kappa - \frac{2\mu}{3}\right)\left(\frac{\partial v_x}{\partial x} + \frac{\partial v_y}{\partial y} + \frac{\partial v_z}{\partial z}\right) + 2\mu \frac{\partial v_z}{\partial y}$$

$$\frac{\partial \sigma_{xy}}{\partial t} = \mu\left(\frac{\partial v_x}{\partial y} + \frac{\partial v_y}{\partial x}\right)$$

$$\frac{\partial \sigma_{xz}}{\partial t} = \mu\left(\frac{\partial v_x}{\partial z} + \frac{\partial v_z}{\partial x}\right)$$

$$\frac{\partial \sigma_{yz}}{\partial t} = \mu\left(\frac{\partial v_y}{\partial z} + \frac{\partial v_z}{\partial y}\right)$$

Equivalently, the stress terms of Equation (2) can be written in terms of strain ($\dot{\varepsilon}_{xx}$, $\dot{\varepsilon}_{yy}$, $\dot{\varepsilon}_{zz}$, $\dot{\varepsilon}_{xy}$, $\dot{\varepsilon}_{xz}$, $\dot{\varepsilon}_{yz}$) and stress as shown in Equation (3).

$$\sigma_{xx} = \left(\kappa - \frac{2\mu}{3}\right)\left(\varepsilon_{xx} + \varepsilon_{yy} + \varepsilon_{zz}\right) + 2\mu\varepsilon_{xx}$$

$$\sigma_{yy} = \left(\kappa - \frac{2\mu}{3}\right)\left(\varepsilon_{xx} + \varepsilon_{yy} + \varepsilon_{zz}\right) + 2\mu\varepsilon_{yy}$$

$$\sigma_{zz} = \left(\kappa - \frac{2\mu}{3}\right)\left(\varepsilon_{xx} + \varepsilon_{yy} + \varepsilon_{zz}\right) + 2\mu\varepsilon_{zz} \qquad \textbf{(3)}$$

$$\sigma_{xy} = 2\mu\varepsilon_{xy}$$

$$\sigma_{xz} = 2\mu\varepsilon_{xz}$$

$$\sigma_{yz} = 2\mu\varepsilon_{yz}$$

To introduce an anelastic effect, it is enough to add an anelastic term ζ in Equation (3), which gives Equation (4).

$$\sigma_{xx} = \left(\kappa - \frac{2\mu}{3}\right)\left(\varepsilon_{xx} + \varepsilon_{yy} + \varepsilon_{zz}\right) + 2\mu\varepsilon_{xx} - \xi_{xx}$$

$$\sigma_{yy} = \left(\kappa - \frac{2\mu}{3}\right)\left(\varepsilon_{xx} + \varepsilon_{yy} + \varepsilon_{zz}\right) + 2\mu\varepsilon_{yy} - \xi_{yy}$$

$$\sigma_{zz} = \left(\kappa - \frac{2\mu}{3}\right)\left(\varepsilon_{xx} + \varepsilon_{yy} + \varepsilon_{zz}\right) + 2\mu\varepsilon_{zz} - \xi_{zz} \qquad \textbf{(4)}$$

$$\sigma_{xy} = 2\mu\varepsilon_{xy} - \xi_{xy}$$

$$\sigma_{xz} = 2\mu\varepsilon_{xz} - \xi_{xz}$$

$$\sigma_{yz} = 2\mu\varepsilon_{yz} - \xi_{yz}$$

In the following, the method proposed by Day (1998) and Day and Bradley (2001) to obtain a formulation of this anelastic term ξ is exposed.

Denoting M(t) the time-dependent modulus, the stress can be written as Equation (5).

$$\sigma(t) = \int_0^t M(t - t')d\varepsilon(t') \qquad \textbf{(5)}$$

The unrelaxed modulus M_u, the relaxed modulus M_R, the relaxation of the modulus δM and the normalized relaxation function φ are defined by Equation (6).

$$M_u = M(0)$$

$$M_R = M(\infty) \qquad \textbf{(6)}$$

$$\delta M = M_u - M_R$$

$$M(t) = M_R + \delta M\varphi(t)$$

Following Nowick and Berry (1972), the relaxation function φ(t) can be written in terms of a relaxation spectrum ψ as Equation (7).

$$\varphi(t) = \int_{-\infty}^{\infty} e^{-t/\tau}\Phi(\ln\tau)d(\ln\tau) \qquad \textbf{(7)}$$

The continuous relaxation spectrum is approximated with a discrete spectrum in Equation (8), where τ_i is a relaxation time, λ_i is the relative strength of the corresponding relaxation, and N is the number of relaxation terms in the approximation.

$$\Phi(\ln\tau) \approx \sum_{i=1}^{N} \lambda_i \delta(\ln\tau - \ln\tau_i) \qquad \textbf{(8)}$$

These equations are equivalent to the stress-strain relationship in Equation (9), in which the ζ_i, i = 1,é ,N are memory variables that evolve according to the N first-order differential Equations (10). The corresponding approximation to $Q^{-1}(\omega)$ is given in Equation (11).

$$\sigma(t) = M_u \left[\varepsilon(t) - \sum_{i=1}^{N} \zeta_i(t) \right] \qquad \textbf{(9)}$$

$$\tau_i \frac{\partial \zeta_i(t)}{\partial t} + \zeta_i(t) = \lambda_i \frac{\delta M}{M_u} \varepsilon(t) \qquad \textbf{(10)}$$

$$Q^{-1}(\omega) \approx \frac{\delta M}{M_u} \sum_{i=1}^{N} \frac{\lambda_i \omega \tau_i}{\omega^2 \tau_i^{\,2} + 1} \qquad \textbf{(11)}$$

In the conventional memory variables approach, N memory variables ζ_i are used and 2N values of τ_i and λ_i are chosen in such a way that the above equation is a good approximation to some target $Q^{-1}(\omega)$. However, this method requires important additional storage, compared with the elastic case.

Therefore, Day (1998) proposed an alternative: the idea is to use only a single memory variable at each point and to permit the relaxation time $\tau(x, y, z)$ and the weighting function w(x, y, z) to vary over a fast spatial scale (i.e. the scale length of the variations is shorter than the minimum wavelength of the wave field but larger than the computational unit cell size of the spatial discretization).

When this weighted spatial dependence is introduced into the relaxation equation, it becomes Equation (12), where w is the weighting function.

$$\tau(x, y, z) \frac{\partial \zeta(x, y, z, t)}{\partial t} + \zeta(x, y, z, t) = w(x, y, z) \frac{\delta M}{M_u} \varepsilon(x, y, z, t) \qquad \textbf{(12)}$$

The stress is then the sum of the elastic response plus a single memory term ζ, as in Equation (13).

$$\sigma(x, y, z, t) = M_u \left[\varepsilon(x, y, z, t) - \zeta(x, y, z, t) \right] \qquad \textbf{(13)}$$

Mean stress $\bar{\sigma}$, deviatoric stresses σ_{ij}', volumetric strain ε_{kk} and deviatoric strains ε_{ij}' are defined by Equation (14).

$$\bar{\sigma} = \frac{1}{3}\left(\sigma_{xx} + \sigma_{yy} + \sigma_{zz}\right)$$

$$\sigma_{ij}' = \sigma_{ij} - \bar{\sigma}\delta_{ij} \qquad \textbf{(14)}$$

$$\varepsilon_{kk} = \varepsilon_{xx} + \varepsilon_{yy} + \varepsilon_{zz}$$

$$\varepsilon_{ij}' = \varepsilon_{ij} - \frac{1}{3}\left(\varepsilon_{xx} + \varepsilon_{yy} + \varepsilon_{zz}\right)\delta_{ij}$$

New versions of Equations (12) and (13) are written for mean stress $\bar{\sigma}$, in terms of volumetric strain ε_{kk} and associated memory variable $\bar{\zeta}$, and for deviatoric stresses σ_{ij}' in terms of deviatoric strains ε_{ij}' and associated memory variables ζ_{ij}' as Equations (15) and (16).

$$\tau \frac{\partial \bar{\zeta}}{\partial t} + \bar{\zeta} = w\frac{\delta\kappa}{\kappa_u}\varepsilon_{kk} \qquad \textbf{(15)}$$

$$\tau \frac{\partial \zeta_{ij}'}{\partial t} + \zeta_{ij}' = w\frac{\delta\mu}{\mu_u}\varepsilon_{ij}'$$

$$\bar{\sigma} = \kappa_u\left[\varepsilon_{kk} - \bar{\zeta}\right] \qquad \textbf{(16)}$$

$$\sigma_{ij}' = 2\mu_u\left[\varepsilon_{ij}' - \zeta_{ij}'\right]$$

New variables ξ_{ij} are defined as Equation (17).

$$\xi_{ij} = 2\mu_u\zeta_{ij}' + \kappa_u\bar{\zeta} \qquad \textbf{(17)}$$

These new variables verify Equations (18) and (19).

$$\tau \frac{\partial \xi_{ij}}{\partial t} + \xi_{ij} = w\left[2\delta\mu\varepsilon_{ij} + \left(\delta\kappa - \frac{2\delta\mu}{3}\right)\varepsilon_{kk}\delta_{ij}\right] \qquad \textbf{(18)}$$

$$\sigma_{ij} = 2\mu_u\varepsilon_{ij} + \left(\kappa_u - \frac{2\mu_u}{3}\right)\varepsilon_{kk} - \xi_{ij} \qquad \textbf{(19)}$$

Following Day (1998), N is chosen equal to 8. Then $\tau(x,y,z)$ takes the eight different values τ_k, k = 1,é ,8, which are assigned to the grid node points in a periodic array. The eight values of w(x,y,z), w_k, are given by the eight relaxation strength ə$_k$ and have been normalized to have unit volumetric mean, which implies w_k = 8ə$_k$. The τ_k are supposed to be equally spaced on a logarithmic scale between τ_m and τ_M. All weights w_k are set to 1. Q_{P0} and Q_{S0} then satisfy Equations (20) around a reference frequency ϑ$_0$.

$$Q_{P_0}^{-1} \approx \frac{\pi\delta\left(\kappa+\frac{4}{3}\mu\right)}{2\left(\kappa+\frac{4}{3}\mu\right)_u}\left[\ln\left(\frac{\tau_M}{\tau_m}\right)+\frac{\delta\left(\kappa+\frac{4}{3}\mu\right)}{\left(\kappa+\frac{4}{3}\mu\right)_u}\ln(\varpi_0\tau_m)\right]^{-1} \qquad \textbf{(20)}$$

$$Q_{S_0}^{-1} \approx \frac{\pi\delta\mu}{2\mu_u}\left[\ln\left(\frac{\tau_M}{\tau_m}\right)+\frac{\delta\mu}{\mu_u}\ln(\varpi_0\tau_m)\right]^{-1}$$

Using these expressions of Q_{P0} and Q_{S0}, the new set of Equations (21) and (22) is finally obtained.

$$\tau\frac{\partial\xi_{ij}}{\partial t}+\xi_{ij} = w\left[2\mu_u A_S\varepsilon_{ij}+\left[\left(\kappa_u+\frac{4}{3}\mu_u\right)A_P-2\mu_u A_S\right]\varepsilon_{kk}\delta_{ij}\right] \qquad \textbf{(21)}$$

$$\sigma_{ij} = 2\mu_u\varepsilon_{ij}+\left(\kappa_u-\frac{2}{3}\mu_u\right)\varepsilon_{kk}\delta_{ij}-\xi_{ij} \qquad \textbf{(22)}$$

A_P and A_S are constants that scale with Q_{P0}^{-1} and Q_{S0}^{-1} as in Equation (23), where Q_{P0} and Q_{S0} are the Q values at the reference frequency ϑ$_0$.

$$A_P = \frac{2}{\pi}Q_{P_0}^{-1}\left(\ln\frac{\tau_M}{\tau_m}\right)\left[1-\frac{2}{\pi}Q_{P_0}^{-1}(\ln\omega_0\tau_m)\right]^{-1} \qquad \textbf{(23)}$$

$$A_S = \frac{2}{\pi}Q_{S_0}^{-1}\left(\ln\frac{\tau_M}{\tau_m}\right)\left[1-\frac{2}{\pi}Q_{S_0}^{-1}(\ln\omega_0\tau_m)\right]^{-1}$$

The Equations (21) and (22) give Equations (24) and (25) upon differentiating by time.

$$\tau\frac{\partial\dot{\xi}_{ij}}{\partial t}+\dot{\xi}_{ij} = w\left[2\mu_u A_S\left(\frac{1}{2}\left(\frac{\partial v_i}{\partial x_j}+\frac{\partial v_j}{\partial x_i}\right)\right)+\left[\left(\kappa_u+\frac{4}{3}\mu_u\right)A_P-2\mu_u A_S\right]\frac{\partial v_k}{\partial x_k}\delta_{ij}\right] \qquad \textbf{(24)}$$

$$\frac{\partial \sigma_{ij}}{\partial t} = 2\mu_u \left(\frac{1}{2}\left(\frac{\partial v_i}{\partial x_j} + \frac{\partial v_j}{\partial x_i} \right) \right) + \left(\kappa_u - \frac{2}{3}\mu_u \right) \frac{\partial v_k}{\partial x_k} \delta_{ij} - \dot{\xi}_{ij} \qquad \textbf{(25)}$$

Each unit cell is assigned one of eight relaxation times τ_k and one of the eight associated weights w_k, distributed according to the following scheme (see Figure 1). Grid unit cells are indexed by the three integers *p*, *q*, *r*, such that a reference point in each cell centre is located at vector position $\mathbf{x}_{pqr} = p\mathbf{a}_1 + q\mathbf{a}_2 + r\mathbf{a}_3$, where $\mathbf{a}_1$, $\mathbf{a}_2$, $\mathbf{a}_3$ are the lattice vectors of the grid. Then the cell $\mathbf{x}_{pqr}$ is assigned τ_k and w_k, where k follows Equation (26).

$$k = 1 + p \bmod 2 + 2(q \bmod 2) + 4(r \bmod 2) \qquad \textbf{(26)}$$

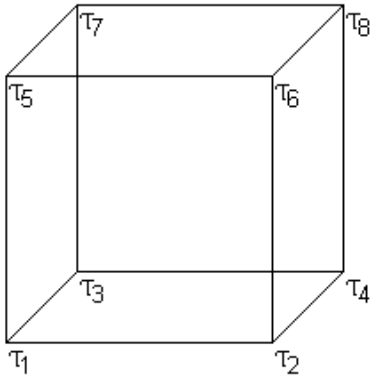

Figure 1 – Indexation of relaxation times τ_k associated to finite differences grid cells for the method of Day and Bradley.

The equation of evolution of memory variable ξ is then rewritten as Equations (27) and (28).

$$\dot{\xi}(t+\delta t) = \frac{\left(\tau_k / \delta t - \frac{1}{2} \right) \dot{\xi}(t) + \frac{1}{2}\left[f(t) + f(t+\delta t) \right]}{\left(\tau_k / \delta t + \frac{1}{2} \right)} \qquad \textbf{(27)}$$

$$f(t) = w_k \left\{ 2\mu_u A_S \left(\frac{1}{2}\left(\frac{\partial v_i(t)}{\partial x_j} + \frac{\partial v_j(t)}{\partial x_i} \right) \right) + \left[\left(\kappa_u + \frac{4}{3}\mu_u \right) A_P - 2\mu_u A_S \right] \frac{\partial v_l}{\partial x_l} \delta_{ij} \right\} \qquad \textbf{(28)}$$

Following Day (1998), τ_k is taken as Equation (29), with all weights equal to 1.

$$\ln(\tau_k) = \ln(\tau_m) + \frac{2k-1}{16}\left(\ln(\tau_M) - \ln(\tau_m)\right) \quad \textbf{(29)}$$

Day and Bradley (2001) propose to take $\tau_m = \varpi_n^{-1}$ and $\tau_M = 5N_t\varpi_n^{-1}$, where ϖ_n is the Nyquist frequency associated with the computational time step and N_t is the total number of time steps in the computation.

2.1.2. Implementation in the 3D code

a) Grid cell

A classical staggered grid in space and time (Madariaga, 1976, and Virieux, 1986) is used (Figure 2).

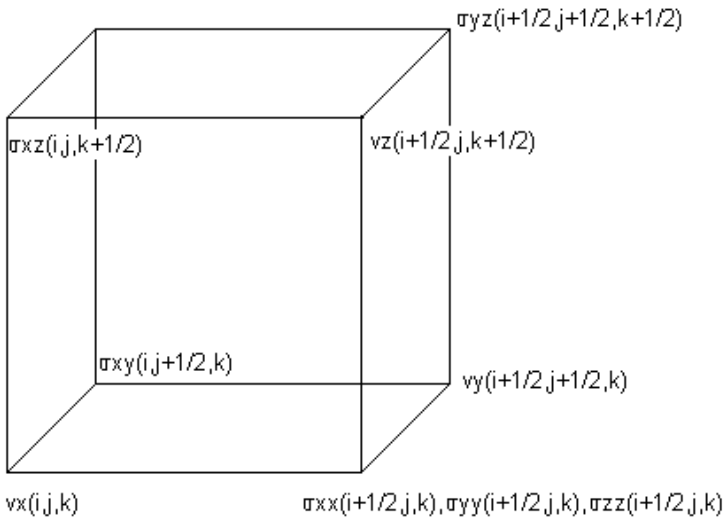

Figure 2 – Elementary grid cell used classically to discretize the equations of elastodynamics.

b) Absorbing boundaries (CPML)

To simulate artificial absorbing boundaries a CPML condition is implemented in the computational code.

The CPML condition was developed in the elastic case by Collino and Tsogka (2001) and Komatitsch and Martin (2007). The technique used is the following: in the regular computational domain, the seismic elastic wave equation has plane wave solutions of the form $\vec{A}\exp\left(-i\left(\vec{k}.\vec{x} - \omega t\right)\right)$.

Let us consider a CPML layer located in x > 0 and the regular domain located in x Ò0. In the regular domain, the seismic elastic wave equation remains unchanged. But, in

the CPML layer, the wave equation is transformed in order to have a plane wave solution which amplitude decreases exponentially in x.

First, a damping profile $d_x(x)$ is defined in the CPML region, such that $d_x = 0$ inside the regular domain and $d_x > 0$ in the CPML, and two other variables $\kappa_x(x)$ and $\alpha_x(x)$, such that $\kappa_x = 0$ and $\alpha_x = 1$ inside the regular domain and κ_x Ó0 and α_x Ó1 in the CPML.

Komatitsch and Martin (2007) showed that we simply need to introduce a new variable $\tilde{x}$ and rewrite the seismic elastic wave equation in terms of $\tilde{x}$ instead of x to have an equation which will have a plane wave solution in the regular domain and a plane wave solution which amplitude decrease exponentially in x in the CPML.

The $\frac{\partial}{\partial x}$ derivative is then replaced in the seismic elastic wave equation by the $\frac{\partial}{\partial \tilde{x}}$ derivative, which can be expressed at time n + ½ by Equation (30), where variables $\acute{u}_x$, b_x and a_x are given in Equation (31).

$$\left.\frac{\partial}{\partial \tilde{x}}\right|_{n+\frac{1}{2}} = \frac{1}{\kappa_x}\left.\frac{\partial}{\partial x}\right|_{n+\frac{1}{2}} + \varphi_x{}^n \qquad \textbf{(30)}$$

$$\varphi_x{}^n = b_x \varphi_x{}^{n-1} + a_x \left(\frac{\partial}{\partial x}\right)^{n+\frac{1}{2}}$$

$$b_x = \exp\left(-\left(d_x/\kappa_x + \alpha_x\right)\Delta t\right) \qquad \textbf{(31)}$$

$$a_x = \frac{d_x}{\kappa_x\left(d_x + \kappa_x \alpha_x\right)}\left(b_x - 1\right)$$

In the anelastic case, we simply need to modify our equations and, wherever we find the derivative $\frac{\partial}{\partial x}$, we replace it in the CPML layer by $\frac{\partial}{\partial \tilde{x}} = \frac{1}{\kappa_x}\frac{\partial}{\partial x} + \varphi_x$. We use then the same technique for all the boundaries were we want to have no reflection.

c) Boundary conditions

Absorbing boundaries at $x = x_{min}$, $x = x_{max}$, $y = y_{min}$, $y = y_{max}$ and $z = z_{min}$ and a free surface at $z = z_{max} = 0$ are implemented. The former tells a fixed boundary condition outside of CPML layer, given in Equations (32), where i_{min}, i_{max}, j_{min}, j_{max} and k_{min} are the limits of the regular domain and œis the number of cells in the CPML layer.

$$
\begin{aligned}
&v_x\left(i_{\min}-\Delta,.,.\right)=0\\
&v_x\left(i_{\max}+\Delta,.,.\right)=0\\
&v_x\left(.,j_{\min}-\Delta,.\right)=0\\
&v_x\left(.,j_{\max}+\Delta,.\right)=0\\
&v_x\left(.,.,k_{\min}-\Delta\right)=0
\end{aligned}
$$

$$
\begin{aligned}
&v_y\left(i_{\min}-\Delta+1/2,.,.\right)=0\\
&v_y\left(i_{\max}+\Delta+1/2,.,.\right)=0\\
&v_y\left(.,j_{\min}-\Delta+1/2,.\right)=0\\
&v_y\left(.,j_{\max}+\Delta+1/2,.\right)=0\\
&v_y\left(.,.,k_{\min}-\Delta\right)=0
\end{aligned}
\qquad \textbf{(32)}
$$

$$
\begin{aligned}
&v_z\left(i_{\min}-\Delta+1/2,.,.\right)=0\\
&v_z\left(i_{\max}+\Delta+1/2,.,.\right)=0\\
&v_z\left(.,j_{\min}-\Delta,.\right)=0\\
&v_z\left(.,j_{\max}+\Delta,.\right)=0\\
&v_z\left(.,.,k_{\min}-\Delta+1/2\right)=0
\end{aligned}
$$

At the free surface, the stress-imaging condition proposed by Graves (1996) is used.

d) Moment source

A generalized moment-tensor source, which uses a distribution of body forces that are added to the individual components of velocity (Graves, 1996), is implemented in ONDES3D.

2.2. METHOD OF KRISTEK AND MOCZO

The second anelasticity method implemented in ONDES3D was proposed by Moczo *et al*. (2002) and Kristek and Moczo (2003). As in the Day and Bradley method, anelastic behaviour is taken into account by introducing anelastic terms in the wave equation for elastic method. Its theoretical formulation and how it was implemented in the code are exposed hereafter.

2.2.1. Theoretical formulation

Anelastic functions $\zeta_l^{M,ij}$, with M = ə, ε , and l = 1, 2, é , n, are introduced and the wave equation becomes Equation (33).

$$\frac{\partial \sigma_{ij}}{\partial t} = \kappa \dot{\varepsilon}_{kk} \delta_{ij} + 2\mu \left(\dot{\varepsilon}_{ij} - \frac{1}{3} \dot{\varepsilon}_{kk} \delta_{ij} \right) - \sum_{l=1}^{n} \left[\kappa \dot{\zeta}_l^{\kappa,kk} \delta_{ij} + 2\mu \left(\dot{\zeta}_l^{\mu,ij} - \frac{1}{3} \dot{\zeta}_l^{\mu,kk} \delta_{ij} \right) \right] \quad \textbf{(33)}$$

The $\zeta_l^{M,ij}$ satisfy the 9n Equations (34), where the τ_l, l = 1, 2, é , n, are angular relaxation frequencies.

$$\ddot{\zeta}_l^{M,ij} + \omega_l \dot{\zeta}_l^{M,ij} = \omega_l Y_l^M \dot{\varepsilon}_{ij} \quad \textbf{(34)}$$

n values of τ_l and k = 2n - 1 values of $\tilde{\omega}_k$, where the k values of quality factor $\tilde{Q}_\eta(\tilde{\omega}_k)$ are imposed, are chosen. The values of anelastic coefficients Y_l^η are then obtained from the system of Equations (35), where k = 1, 2, é , 2n ï 1 and ç = Ü, ß.

$$\sum_{l=1}^{n} \frac{\omega_l \tilde{\omega}_k + \omega_l^2 \tilde{Q}_\eta^{-1}(\tilde{\omega}_k)}{\tilde{\omega}_k^2 + \omega_l^2} Y_l^\eta = \tilde{Q}_\eta^{-1}(\tilde{\omega}_k) \quad \textbf{(35)}$$

Anelastic coefficients Y_l^κ and Y_l^μ are then given by Equations (36) and (37).

$$Y_l^\mu = Y_l^\beta \text{ and } Y_l^\kappa = \frac{\alpha^2 Y_l^\alpha - \frac{4}{3}\beta^2 Y_l^\beta}{\alpha^2 - \frac{4}{3}\beta^2} \quad \textbf{(36)}$$

$$\alpha = \left[\left(\kappa + \frac{4}{3}\mu \right) \Big/ \rho \right]^{1/2} \textit{ and } \beta = (\mu/\rho)^{1/2} \quad \textbf{(37)}$$

Variables ξ_l are defined by Equations 38.

$$\xi_l^{ij} = \kappa \zeta_l^{\kappa,kk} \delta_{ij} + 2\mu \left(\zeta_l^{\mu,ij} - \frac{1}{3} \zeta_l^{\mu,kk} \delta_{ij} \right) \quad \textbf{(38)}$$

Equation (32) is then rewritten as Equation (39).

$$\frac{\partial \sigma_{ij}}{\partial t} = \kappa \dot{\varepsilon}_{kk} \delta_{ij} + 2\mu \left(\dot{\varepsilon}_{ij} - \frac{1}{3} \varepsilon_{kk} \delta_{ij} \right) - \sum_{l=1}^{n} \dot{\xi}_l^{ij} \quad \textbf{(39)}$$

There are now 6n anelastic functions, respecting the Equations (40).

$$\ddot{\xi}_l^{ij} + \omega_l \dot{\xi}_l^{ij} = \omega_l \left[\kappa Y_l^\kappa \dot{\varepsilon}_{kk} \delta_{ij} + 2\mu Y_l^\mu \left(\dot{\varepsilon}_{ij} - \frac{1}{3} \dot{\varepsilon}_{kk} \delta_{ij} \right) \right] \quad \textbf{(40)}$$

New anelastic functions are now introduced in Equation (41).

$$\zeta_l^{new,ij} = \zeta_l^{M,ij} \Big/ Y_l^M \qquad \textbf{(41)}$$

These new functions verify Equation (42).

$$\xi_l^{ij} = \kappa Y_l^{\kappa} \zeta_l^{new,kk} \delta_{ij} + 2\mu Y_l^{\mu} \left(\zeta_l^{new,ij} - \frac{1}{3} \zeta_l^{new,kk} \delta_{ij} \right) \qquad \textbf{(42)}$$

They respect the 6n Equations (43), with l = 1, 2, é , n.

$$\dot{\zeta}_l^{new,ij} + \varpi_l \zeta_l^{new,ij} = \varpi_l \dot{\varepsilon}_{ij} \qquad \textbf{(43)}$$

The Equation (38) becomes then equation (44).

$$\frac{\partial \sigma_{ij}}{\partial t} = \kappa \dot{\varepsilon}_{kk} \delta_{ij} + 2\mu \left(\dot{\varepsilon}_{ij} - \frac{1}{3} \dot{\varepsilon}_{kk} \delta_{ij} \right) - \sum_{l=1}^{n} \left[\kappa Y_l^{\kappa} \dot{\zeta}_l^{new,kk} \delta_{ij} + 2\mu Y_l^{\mu} \left(\dot{\zeta}_l^{new,ij} - \frac{1}{3} \dot{\zeta}_l^{new,kk} \delta_{ij} \right) \right] \qquad \textbf{(44)}$$

Equations (45) and (46) are deduced from Equations (42) and (43), where variables $\tilde{\kappa}$, $\tilde{\mu}$, $\tilde{Y}$, $\tilde{Y}_l^{\mu}$, d_l and c_l are given in Equation (47).

$$\dot{\zeta}_l^{new,ij}\left(t_{n+1/2}\right) = \frac{2\varpi_l dt}{2+\varpi_l dt} \dot{\varepsilon}_{ij}\left(t_n\right) + \frac{2-\varpi_l dt}{2+\varpi_l dt} \dot{\zeta}_l^{new,ij}\left(t_{n-1/2}\right) \qquad \textbf{(45)}$$

$$\begin{aligned} \frac{\partial \sigma_{ij}\left(t_n\right)}{\partial t} &= \tilde{\kappa} \dot{\varepsilon}_{kk}\left(t_n\right) \delta_{ij} + 2\tilde{\mu} \left(\dot{\varepsilon}_{ij}\left(t_n\right) - \frac{1}{3} \dot{\varepsilon}_{kk}\left(t_n\right) \delta_{ij} \right) \\ &- \sum_{l=1}^{n} \left[\tilde{Y}_l^{\kappa} \dot{\zeta}_l^{new,kk}\left(t_{n+1/2}\right) \delta_{ij} + 2\tilde{Y}_l^{\mu} \left(\dot{\zeta}_l^{new,ij}\left(t_{n+1/2}\right) - \frac{1}{3} \dot{\zeta}_l^{new,kk}\left(t_{n+1/2}\right) \delta_{ij} \right) \right] \end{aligned} \qquad \textbf{(46)}$$

$$\tilde{\kappa} = \kappa \left(1 + \sum_{l=1}^{n} d_l Y_l^{\kappa} \right) \ , \ \tilde{\mu} = \mu \left(1 + \sum_{l=1}^{n} d_l Y_l^{\mu} \right) \ , \ \tilde{Y} = c_l \kappa Y_l^{\kappa} \ , \ \tilde{Y}_l^{\mu} = c_l \mu Y_l^{\mu} \ , \ d_l = \frac{\varpi_l dt}{2 - \omega_l dt} \ ,$$

$$c_l = \frac{2}{2 - \varpi_l dt} \qquad \textbf{(47)}$$

At time t, the values of $v_i(t)$ are computed from the values of $v_i(t - dt)$ and $\mathring{u}_{ij}(t - dt/2)$.

At time t + dt/2, the values of $\dot{\zeta}_l^{new,ij}\left(t + dt/2\right)$ are first computed from the values of $\dot{\zeta}_l^{new,ij}\left(t - dt/2\right)$ and $v_i(t)$, and then, the values of $\mathring{u}_{ij}(t + dt/2)$ are computed from the values of $\dot{\zeta}_l^{new,ij}\left(t + dt/2\right)$, $\mathring{u}_{ij}(t - dt/2)$ and $v_i(t)$.

For each grid cell, we presently need to keep in memory *l* anelastic variables corresponding to *l* relaxation frequencies. This requires a lot of memory storage; therefore Kristek and Moczo (2003) developed a method where we need only one anelastic variable per grid cell.

The scheme for equation may be symbolically written as Equation (48).

$$\frac{\partial \Sigma_{I,J,K}}{\partial t} = 2\tilde{\mu}_{I,J,K}\dot{V}_{I,J,K} - 2\sum_{l=1}^{4}\tilde{Y}_{l,I,J,K}\dot{X}_{l,I,J,K} \qquad \textbf{(48)}$$

We take n = 4 and, in each grid cell (I,J,K), we compute the anelastic function only for one particular relaxation frequency. We then approximate the sum over l = 1, é , 4 by weighted averaging of the anelastic functions from the grid cell (I,J,K) and neighbouring grid cells (see Figure 3). The Equation scheme (49) gives natural averaging in three coordinate directions.

$$\begin{aligned}\frac{\partial \Sigma_{I,J,K}}{\partial t} &= 2\tilde{\mu}_{I,J,K}\dot{V}_{I,J,K} - 2\tilde{Y}_{ind(I,J,K),I,J,K}\dot{X}_{ind(I,J,K),I,J,K} \\ &- 2\tilde{Y}_{ind(I-1,J,K),I,J,K}\frac{\dot{X}_{ind(I-1,J,K),I-1,J,K} + \dot{X}_{ind(I+1,J,K)I+1,J,K}}{2} \\ &- 2\tilde{Y}_{ind(I,J-1,K),I,J,K}\frac{\dot{X}_{ind(I,J-1,K)I,J-1,K} + \dot{X}_{ind(I,J+1,K),I,J+1,K}}{2} \\ &- 2\tilde{Y}_{ind(I,J,K-1),I,J,K-1}\frac{\dot{X}_{ind(I,J,K-1),I,J,K-1} + \dot{X}_{ind(I,J,K+1)I,J,K+1}}{2}\end{aligned} \qquad \textbf{(49)}$$

The indices *ind*(*I*,*J*,*K*) are defined by Equation (50).

$$\begin{aligned}ind(I,J,K) &= (J \bmod 2)\{1 + (K-1)\bmod 2 + 2[(I-1)\bmod 2]\} \\ &+ (1 - J \bmod 2)\{1 + K \bmod 2 + 2[(I)\bmod 2]\}\end{aligned} \qquad \textbf{(50)}$$

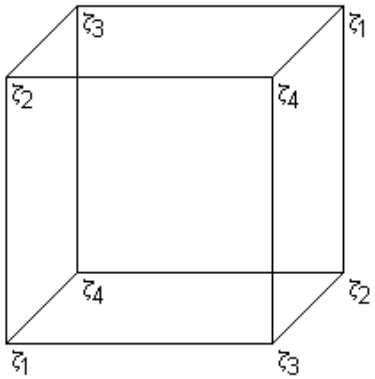

Figure 3 ï Indexation of the finite difference grid cells for the method of Kristek and Moczo.

2.2.2. Implementation in the code

a) Grid cell

The same classical staggered grid in space and time (Madariaga, 1976, and Virieux, 1986) as in the first method is used (See Figure 2).

b) Absorbing boundaries (CPML)

We use the same technique as in the first method (See chapter 2.1). If we consider a CPML layer located in x > 0 and the regular domain located in x Ò0, we simply need to modify our equations and, wherever we find the derivative $\frac{\partial}{\partial x}$, we replace it in the CPML layer by $\frac{\partial}{\partial \tilde{x}} = \frac{1}{\kappa_x}\frac{\partial}{\partial x} + \varphi_x$. We use then the same technique for all the boundaries where we want to have no reflection.

c) Boundary conditions

We use the same technique as in the first method (See chapter 2.1).

d) Moment source

We use the same moment source as in the first method (See chapter 2.1).

3. Numerical tests

In order to test the efficiency of the two anelastic methods implemented in the code ONDES3D and to compare them, several series of tests are carried out. These results were obtained in the context of an internship during year 2009 (Lee-tin-yien, 2009).

3.1. EFFECTS OF THE ANELASTIC PARAMETERS

The aim of the first series of simulations is to test the effects of the anelastic parameters f_m and f_M for the method of Day and Bradley and τ_{min} and τ_{max} for the method of Kristek and Moczo on the results of the computation.

A model setting similar to the one proposed in Day and Bradley (2001) is used. There are CPML boundaries on the six sides of the model, at x = -10 km and x = 10 km, at y = -10 km and y = 10 km, at z = -10 km and z = 10 km. The (x, y, z)-Cartesian coordinates are taken as (east, north, upward). The size of the grid cell is $\delta x = \delta y = \delta z = 100$ m.

The time step is 0.008 s and the simulation is performed for 500 time steps.

The source is located at $x_{source} = 0$, $y_{source} = 0$, $z_{source} = -2$ km.

The moment rate function $\dot{m}(t)$ of the dislocation source is a Gaussian with spread S, given in Equation (51), where *H* is the Heaviside step function, $M_0 = 10^{18}$ N.m and S = 0.045 s.

$$\dot{m}(t) = \frac{M_0 H(t)}{\sqrt{2\pi}\, S} e^{-0.5(t-4S)^2/S^2} \qquad \textbf{(51)}$$

The parameters of the source are strike $\phi = 0$, dip $\delta = \pi/2$ and rake $\lambda = 0$.

The anelasticity parameters are $Q_{S0} = Q_{P0} = 50$. P- and S-wave velocities and density are respectively $V_P = 6000$ m.s^{-1}, $V_S = 3460$ m.s^{-1} and $\rho = 2700$ kg.m^{-3}.

The receiver is located at $x_{receiver} = 8$ km, $y_{receiver} = 6$ km, $z_{receiver} = 0$ km.

Three sets of parameters f_m and f_M for the method of Day and Bradley and three sets of parameters τ_{min} and τ_{max} for the method of Kristek and Moczo are tested (Table 1). The first set of parameters f_m and f_M is taken according to the values proposed by Day and Bradley (2001). For the set of parameters τ_{min} and τ_{max}, we took the inverse frequencies of f_m and f_M.

Simulation number	Parameters for Day and Bradley method		Parameters for Kristek and Moczo method	
	Q_n	Q_M	τ_{min}	τ_{max}
1	0.016	40	$2´/Q_M$ = $2´*0.025$	$2´/Q_n = 2´*62.5$
2	$2´/\tau_{max} = 0.05$	$2´/\tau_{min} = 10$	$2´*0.1$	$2´*20$
3	$0.1*Q_{n2} = 0.005$	$10*Q_{M2} = 100$	$10*\tau_{min1}$ = $2´*0.25$	$0.1*\tau_{max1}$ = $2´*6.25$

Table 1 ï Sets of anelasticity parameters used for the simulations.

Figures 4 to 6 show seismograms of the simulations for each component of the velocity vector for the three sets of parameters for the method of Day and Bradley.

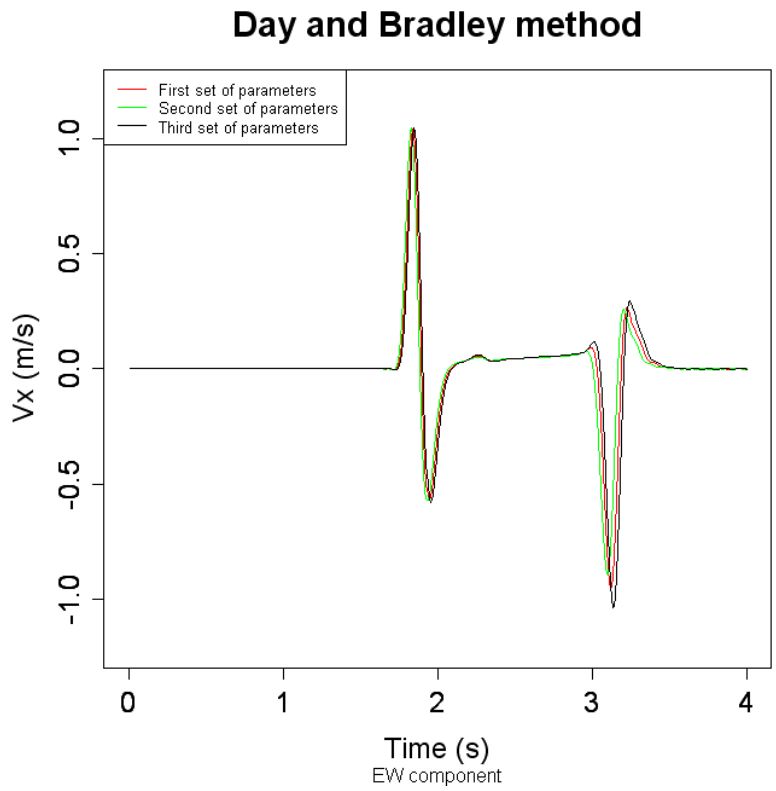

Figure 4 ï EW component of the velocity vector with the method of Day and Bradley for the first set of parameters (red), the second set of parameters (green) and the third set of parameters (black).

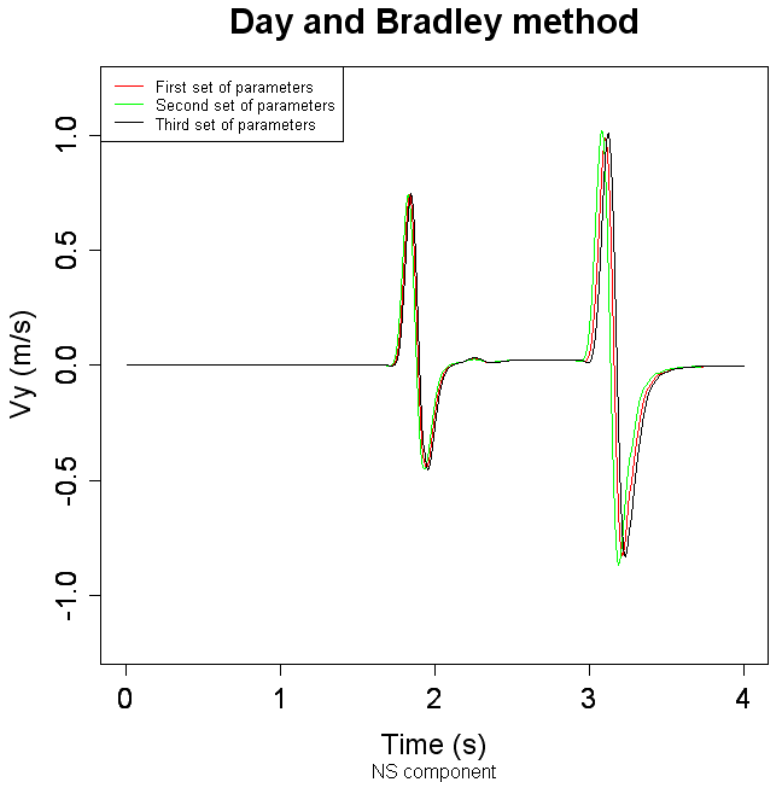

Figure 5 ï NS component of the velocity vector for the method of Day and Bradley for the fisrt set of parameters (red), the second set of parameters (green) and the third set of parameters (black).

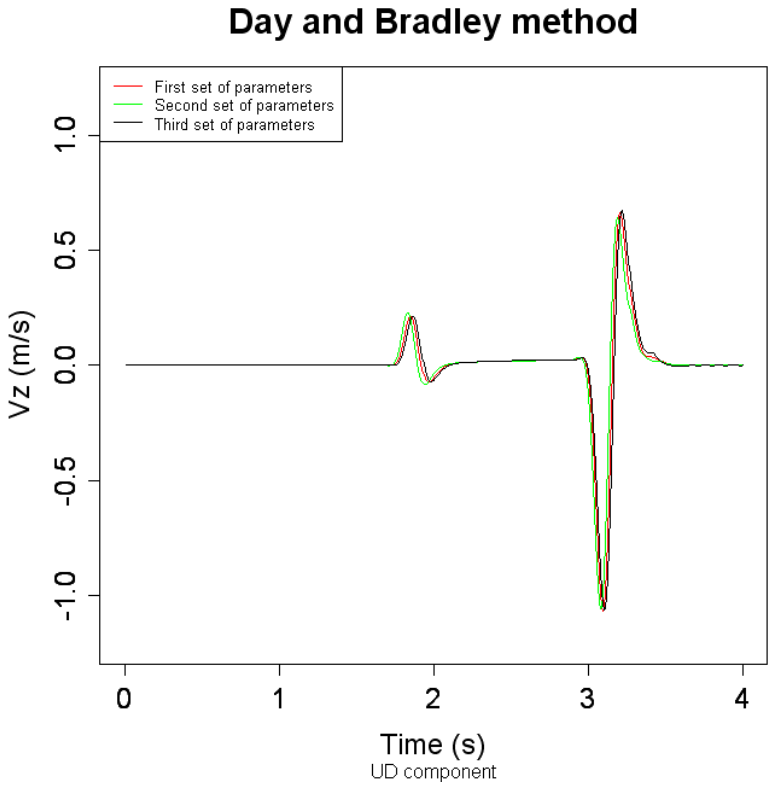

Figure 6 ï UD component of the velocity vector for the method of Day and Bradley with the first set of parameters (red), the second set of parameters (green) and the third set of parameters (black).

The simulations show that the three sets of parameters $\acute{U}_m$ and $\acute{U}_M$ give similar results. Therefore, the set of parameters proposed by Day and Bradley (2001) will be used in the following series of tests.

Figures 7 to 9 show seismograms of the simulations for each component of the velocity vector for the three sets of parameters for the method of Kristek and Moczo.

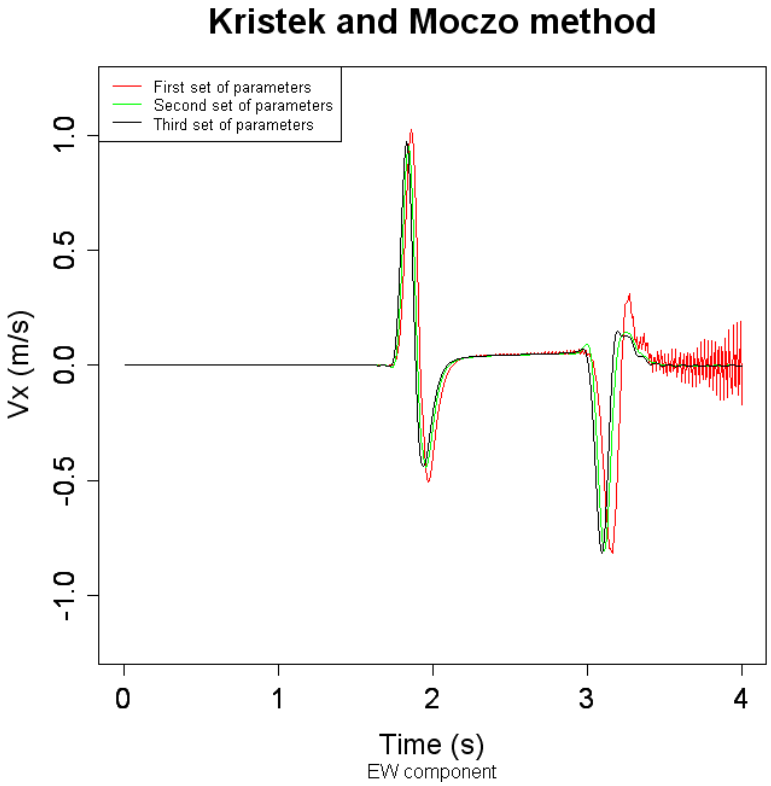

Figure 7 ï EW component of the velocity vector for the method of Kristek and Moczo for the first set of parameters (red), the second set of parameters (green) and the third set of parameters (black).

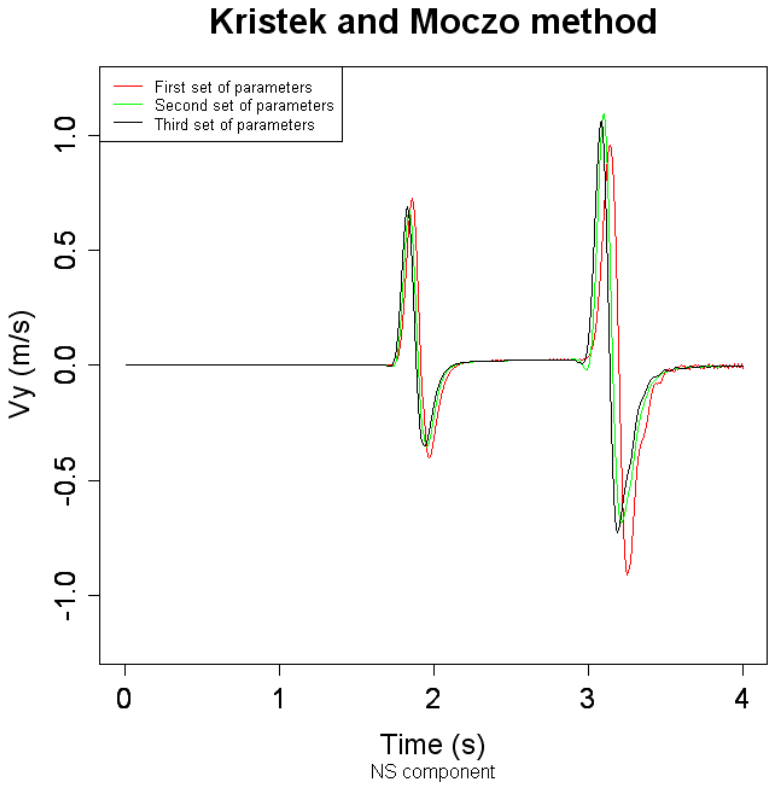

Figure 8 ï NS component of the velocity vector for the method of Kristek and Moczo for the first set of parameters (red), the second set of parameters (green) and the third set of parameters (black).

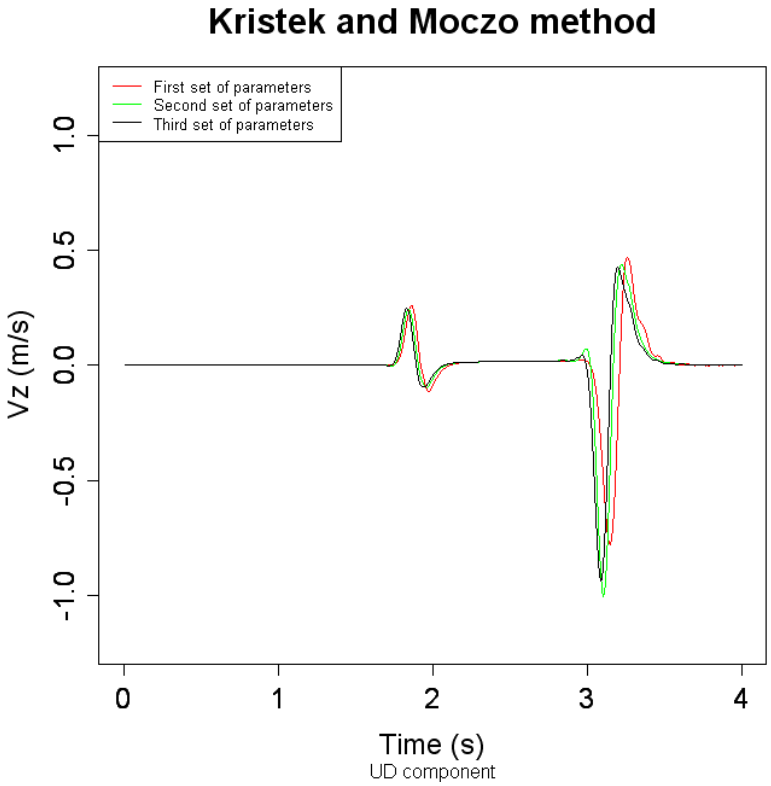

Figure 9 ï UD component of the velocity vector for the method of Kristek and Moczo for the first set of parameters (red), the second set of parameters (green) and the third set of parameters (black).

The simulations show that there is numerical dispersion for the first set of parameters. The third set of parameters seems to give slight better results than the second set of parameters. Indeed, there is a little peak at the beginning of the S-wave which appears with the second set of parameters and not with the third. Therefore, the third set of parameters will be used in the following series of tests.

3.2. TESTING THE FREE SURFACE AND THE CPML

The aim of the second series of simulations is to test the implementation of the free surface.

A model setting similar to the previous one is used. There are CPML boundaries on five sides of the model, at x = -15 km and x = 15 km, at y = -15 km and y = 15 km, at z = -17 km and a free surface at z = 0.

The sets of parameters Q_m and Q_M for the method of Day and Bradley and τ_{min} and τ_{max} for the method of Kristek and Moczo are taken according to the results of the first series of simulations: $Q_m = 0.016$, $Q_M = 40$, $\tau_{min} = 2' *0.25$ and $\tau_{max} = 2' *6.25$.

Figures 10 to 12 show seismograms of the simulations for radial, transverse and vertical components of the velocity vector for the two anelastic methods.

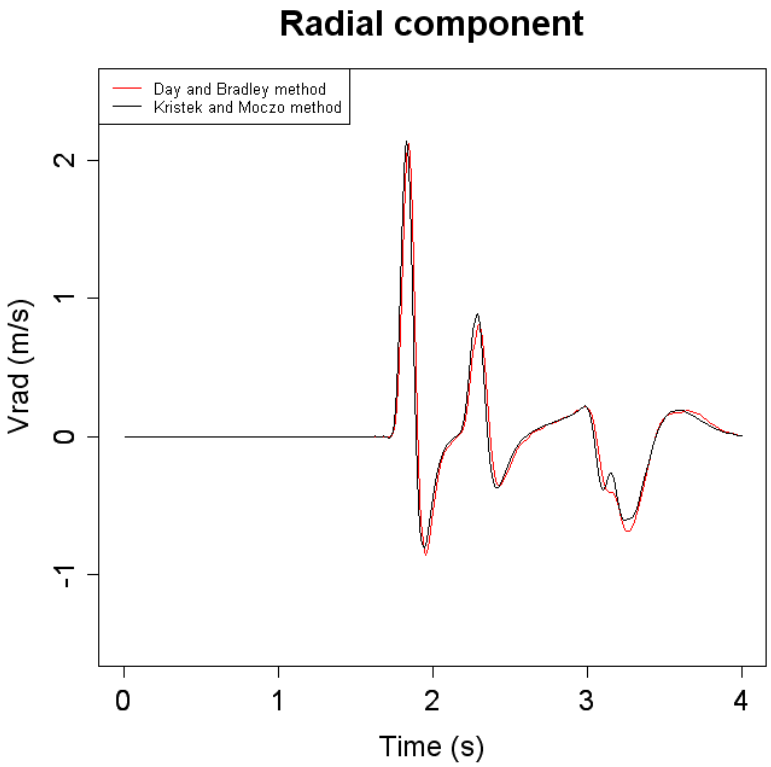

Figure 10 ï Radial component of the velocity vector for the method of Day and Bradley (red) and the method of Kristek and Moczo (black).

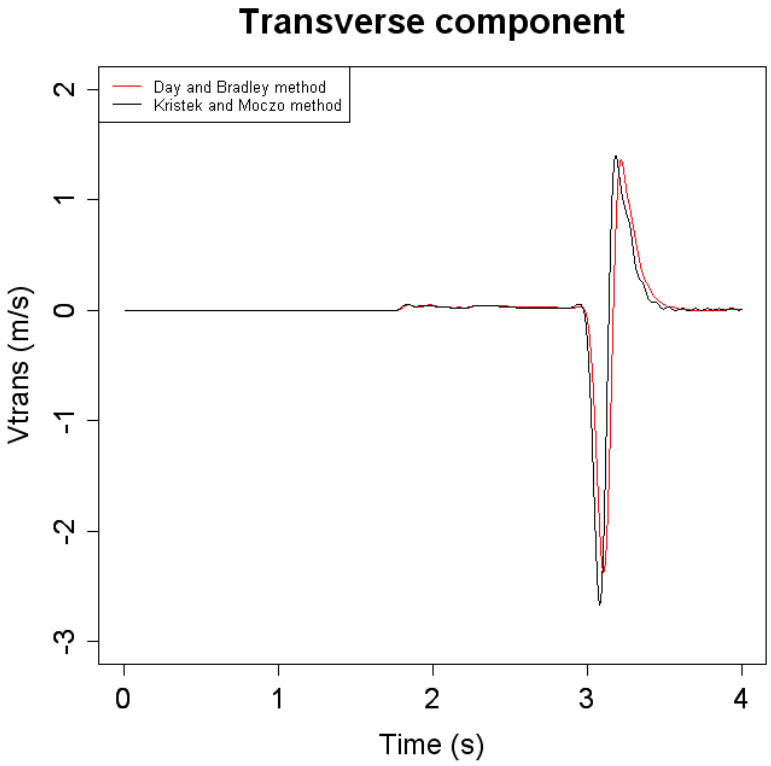

Figure 11 ï Transverse component of the velocity vector for the method of Day and Bradley (red) and the method of Kristek and Moczo (black).

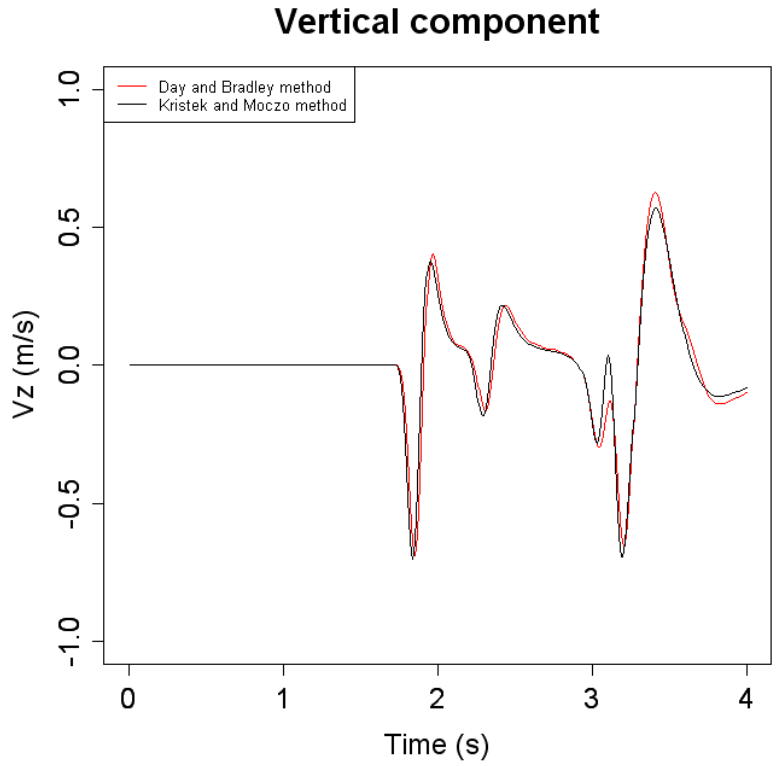

Figure 12 ï Vertical component of the velocity vector for the method of Day and Bradley (red) and the method of Kristek and Moczo (black).

There are slight differences between the two anelastic methods and it is difficult to say which method gives the best results.

A second aim of this series of simulations is to test the efficiency of the CPML. As the boundaries of the model described above are far from the source and the receiver, the model can be considered as infinite. To test the CPML, we compute a simulation with the more difficult case of a smaller model, with boundaries close to the point source and we compare the results with the first model.

In the case of the small model, there are CPML boundaries on five sides of the model, at x = -1 km and x = 15 km, at y = -1 km and y = 15 km, at z = -17 km and a free surface at z = 0 km.

In order to test the efficiency of the CPML at grazing incidence, receivers are added close to the boundaries (Table 2).

Receiver number	x coordinate (km)	y coordinate (km)	z coordinate (km)
1	8000	6000	0

2	8000	100	0
3	14000	100	0

Table 2 ï Coordinates of the receivers

Figures 13 to 15 show seismograms of the simulations for each component of the velocity for the three receivers for the method of Day and Bradley with the small model and the large model.

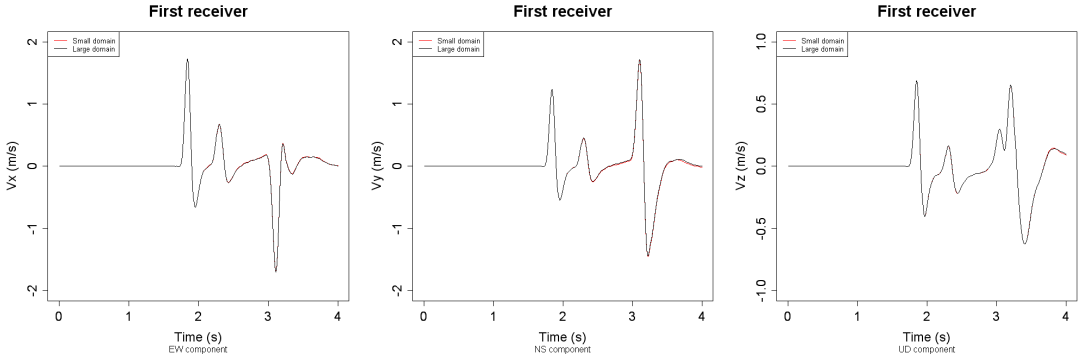

Figure 13 ï EW (left), NS (middle) and UD (right) components of the velocity vector for the first receiver for the small model (red) and the large model (black) for the method of Day and Bradley. For this receiver, there is no grazing incidence and the agreement is almost perfect.

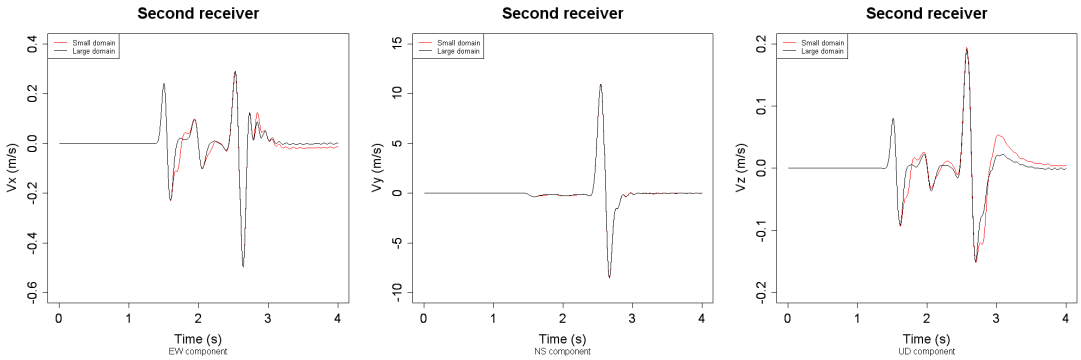

Figure 14 ï EW (left), NS (middle) and UD (right) components of the velocity vector for the second receiver for the small model (red) and the large model (black) for the method of Day and Bradley. For this receiver, with grazing incidence, spurious oscillations start to appear especially for EW and UD components.

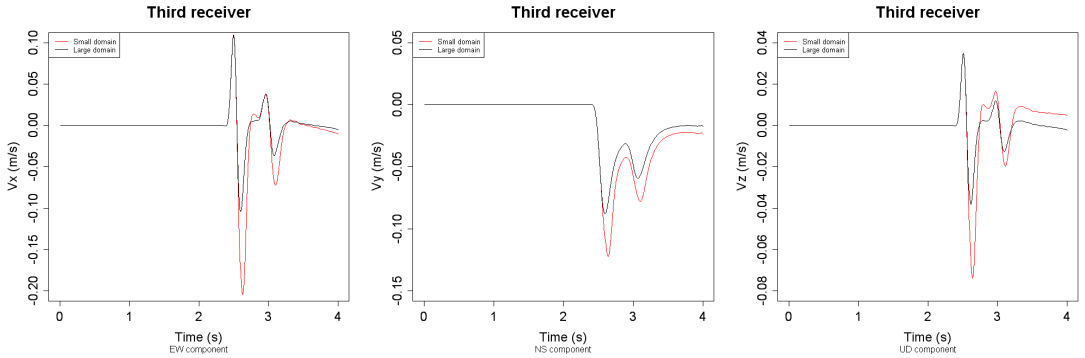

Figure 15 ï EW (left), NS (middle) and UD (right) components of the velocity vector for the third receiver for the small model (red) and the large model (black) for the method of Day and Bradley. For this receiver, with very grazing incidence, the spurious oscillations become large and the signal is completely distorted.

Figures 16 to 18 show seismograms the simulations for each component of the velocity for the three receivers for the method of Kristek and Moczo with the small model and the large model.

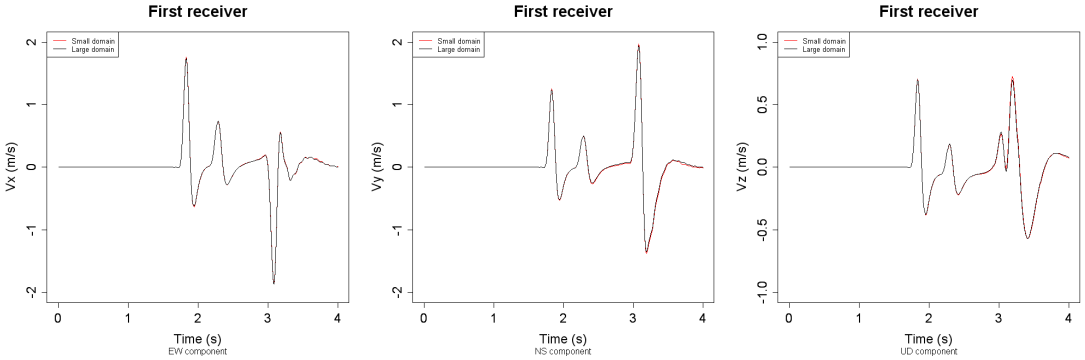

Figure 16 ï EW (left), NS (middle) and UD (right) components of the velocity vector for the first receiver for the small model (red) and the large model (black) for the method of Kristek and Moczo. For this receiver, there is no grazing incidence and the agreement is almost perfect.

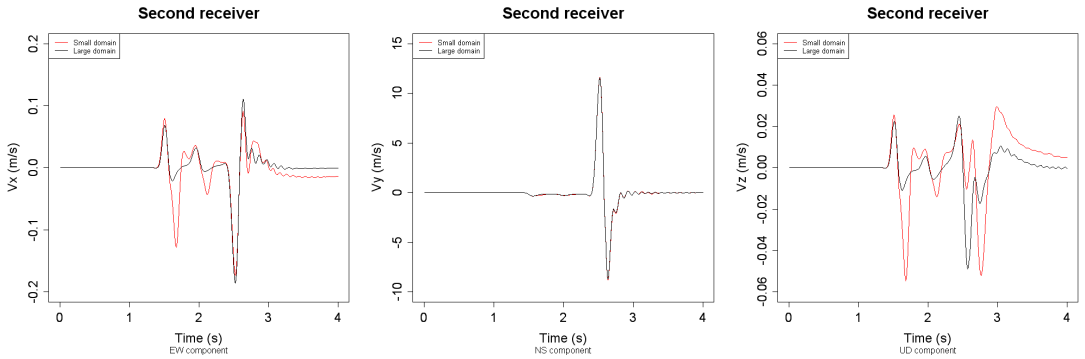

Figure 17 : EW (left), NS (middle) and UD (right) components of the velocity vector for the second receiver for the small model (red) and the large model (black) for the method of Kristek and Moczo. For this receiver, with grazing incidence, the agreement remains good for NS component but spurious oscillations appear for EW and UD components and the signal is completely distorted.

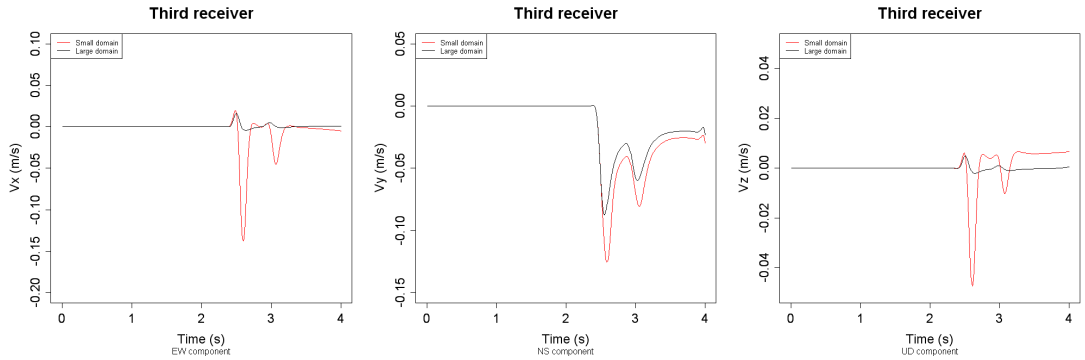

Figure 18 : EW (left), NS (middle) and UD (right) components of the velocity vector for the third receiver for the small model (red) and the large model (black) for the method of Kristek and Moczo. For this receiver, with very grazing incidence, the spurious oscillations become large and the signal is completely distorted.

The CPML gives good results with the method of Day and Bradley. There is a good agreement between the small model and the large model and distortions start to appear only in the case of very grazing incidence. For the method of Kristek and Moczo, the CPML is less efficient. Spurious oscillations start to appear as soon as the incidence is a little grazing.

3.3. EFFICIENCY OF THE TWO METHODS AT DIFFERENT FREQUENCIES

The aim of the two anelastic methods implemented in ONDES3D is to approximate the anelastic quality factor over a specified frequency band. Therefore, it is interesting to check if the quality factor was well approximated in every band of frequency. Moreover, we want to know which method we should use if we want to model more accurately lower or higher frequencies.

The model setting is the problem LOH3 of Day *et al*. (2003) report. There are CPML boundaries on five sides of the model, at x = -15 km and x = 15 km, at y = -15 km and y = 15 km, at z = -17 km and a free surface at z = 0. The (x, y, z)-Cartesian coordinates are taken as (east, north, upward). The size of the grid cell is qx = qy = qz = 100 m.

The time step is 0.008 s and the simulation is performed for 1125 time steps.

The source is located at x_{source} = 0 km, y_{source} = 0 km, z_{source} = - 2 km.

The moment rate function $\dot{m}(t)$ of the dislocation source is given in Equation (52).

$$\dot{m}(t) = M_0 \left(\frac{t}{T^2} \right) e^{-t/T} \qquad \textbf{(52)}$$

The parameters of the moment rate function are $M_0 = 10^{18}$ N.m and T = 0.1 s.

The parameters of the source are strike ű = 0, dip ŭ = ´ /2 and rake ə= 0.

There are two layers of material. The thickness of the top layer is 1000 m. The corresponding anelasticity parameters are Q_{S0} = 40, Q_{P0} = 120. P- and S-wave velocities and density are respectively V_P = 4000 m.s^{-1}, V_S = 2000 m.s^{-1} and ɟ = 2600 kg.m^{-3}.

The anelasticity parameters of the second layer are Q_{S0} = 69.3, Q_{P0} = 155.9. P- and S-wave velocities and density are respectively V_P = 6000 m.s^{-1}, V_S = 3464 m.s^{-1} and ɟ = 2700 kg.m^{-3}.

There are 10 receivers located at $x_{receiver}$ = n * 800 m, $y_{receiver}$ = n * 600 m, $z_{receiver}$ = 0, with n = 1, é , 10.

The anelasticity parameters for the method of Day and Bradley are Ű$_n$ = 0.016 and Ű$_M$ = 90. The parameters for the method of Kristek and Moczo are ϑ $_{min}$ = 0.1 and ϑ $_{max}$ = 10.

To test the accuracy of the two methods at different frequencies, we apply a filter to the computed seismograms. They are convoluted with a Gaussian filter, given in Equation (53).

$$f(t) = \frac{1}{\sqrt{2\pi}\sigma} \left(1 - \frac{2T}{\sigma^2}(t - t_S) - \left(\frac{T}{\sigma} \right)^2 \left(1 - \left(\frac{t - t_S}{\sigma} \right)^2 \right) \right) \exp\left(-\frac{1}{2} \left(\frac{t - t_S}{\sigma} \right)^2 \right) \qquad \textbf{(53)}$$

The parameters of the filter are T = 0.1 and t_S = 4ů.

Three filters are tested: first, a filter with a high rupture frequency (ů = 0.05), then a filter with a lower rupture frequency (ů = 0.1), and finally a filter with a very low rupture frequency (ů = 0.3).

The convoluted seismograms are then compared to the reference solution given by Day *et al.* (2003).

Figures 19 to 21 show the results of the simulations for ů = 0.05 for radial, transverse and vertical components of the velocity vector for the two anelasticity methods.

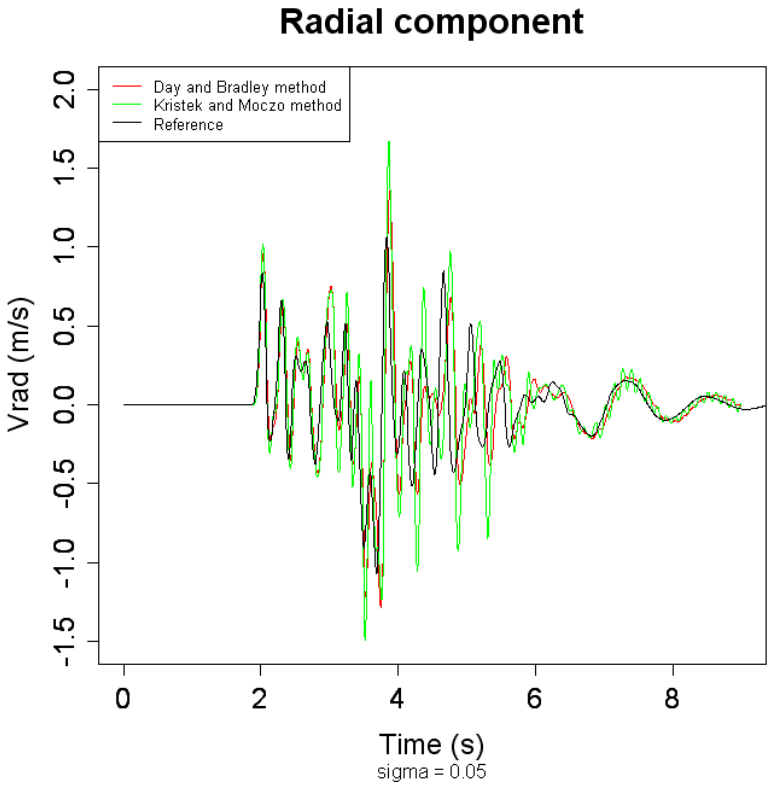

Figure 19 ï Radial component of the velocity vector for ***ů*** *= 0.05 for the method of Day and Bradley (red), for the method of Kristek and Moczo (green) and for the reference solution (black).*

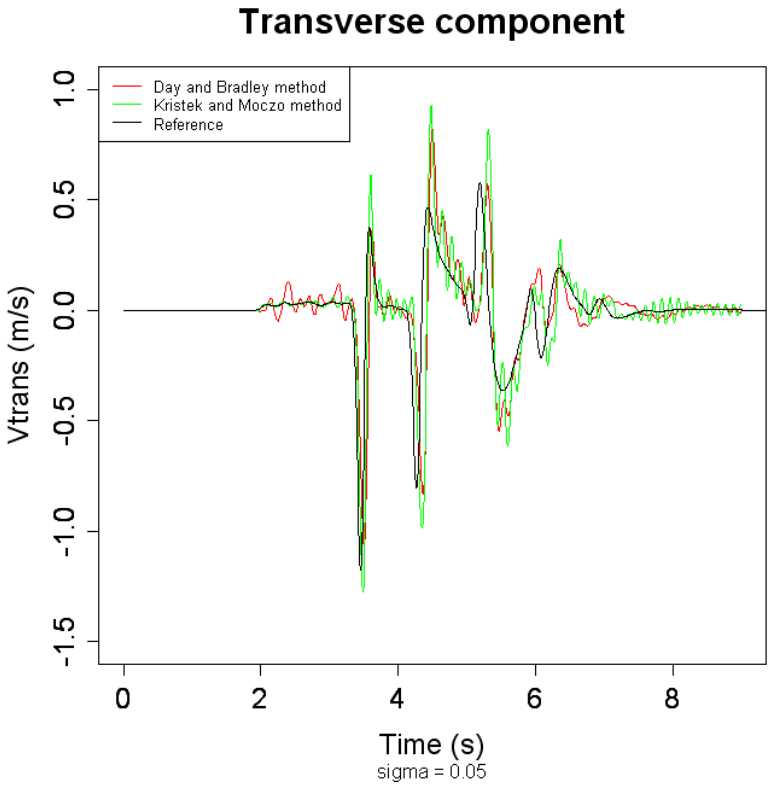

Figure 20 ï Transverse component of the velocity vector for $\sigma = 0.05$ *for the method of Day and Bradley (red), for the method of Kristek and Moczo (green) and for the reference solution (black).*

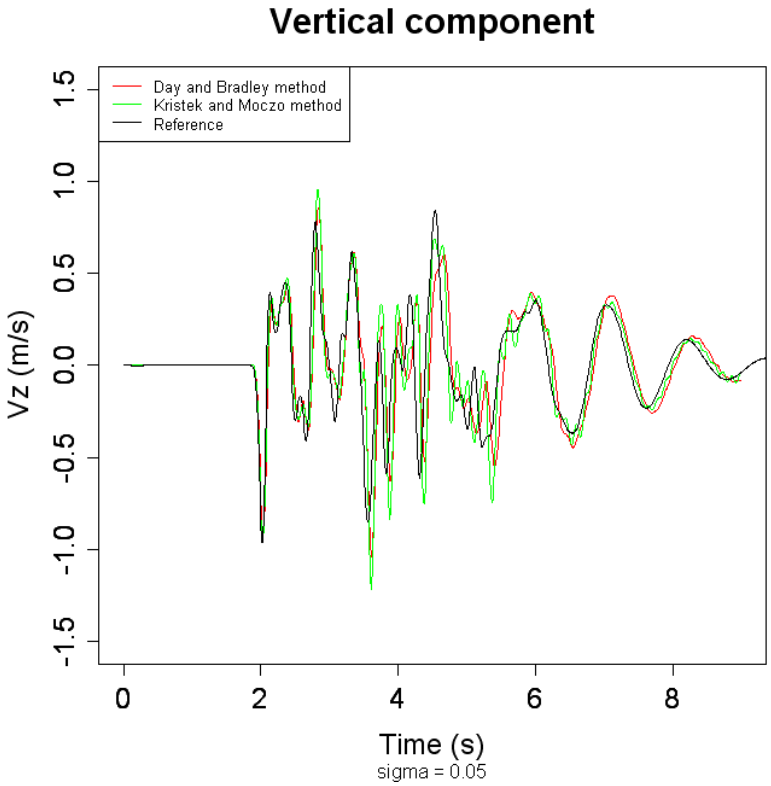

Figure 21 ï Vertical component of the velocity vector for ***ů*** *= 0.05 for the method of Day and Bradley (red), for the method of Kristek and Moczo (green) and for the reference solution (black).*

For the high frequency filter, there is more noise with the method of Kristek and Moczo. However, this method models more accurately the P-wave for the transverse component than the method of Day and Bradley.

Figures 22 to 24 show the results of the simulations for ů = 0.1 for radial, transverse and vertical components of the velocity vector for the two anelasticity methods.

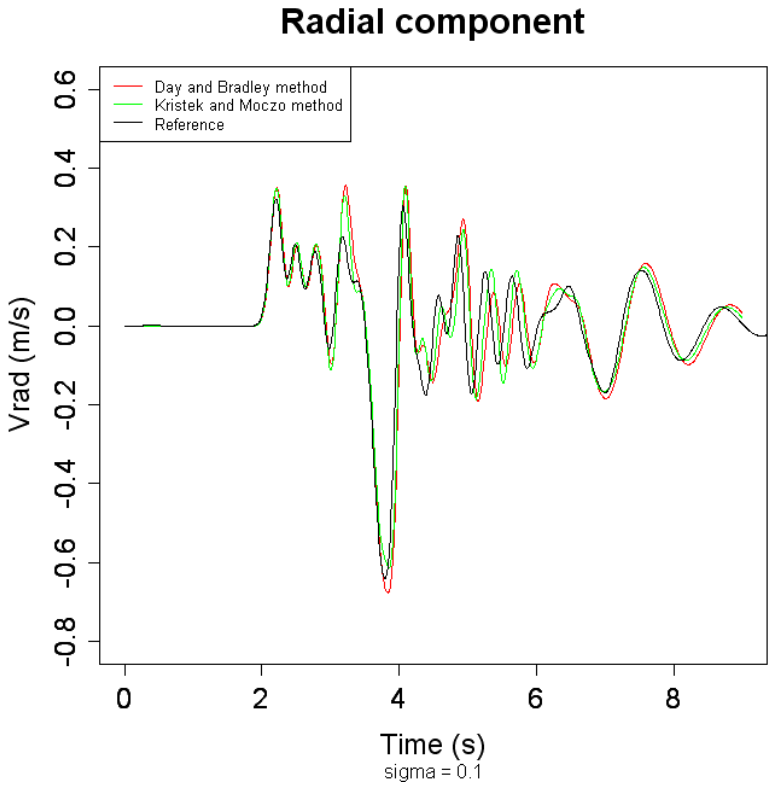

Figure 22 ï Radial component of the velocity vector for ***ů*** *= 0.1 for the method of Day and Bradley (red), for the method of Kristek and Moczo (green) and for the reference solution (black).*

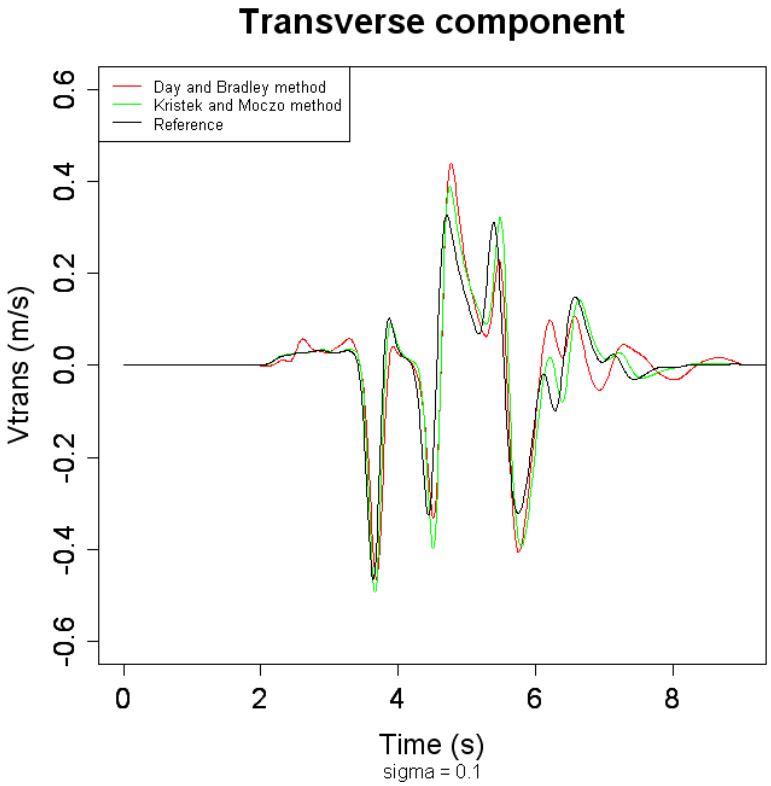

Figure 23 ï Transverse component of the velocity vector for $\mathring{\boldsymbol{u}} = 0.1$ *for the method of Day and Bradley (red), for the method of Kristek and Moczo (green) and for the reference solution (black).*

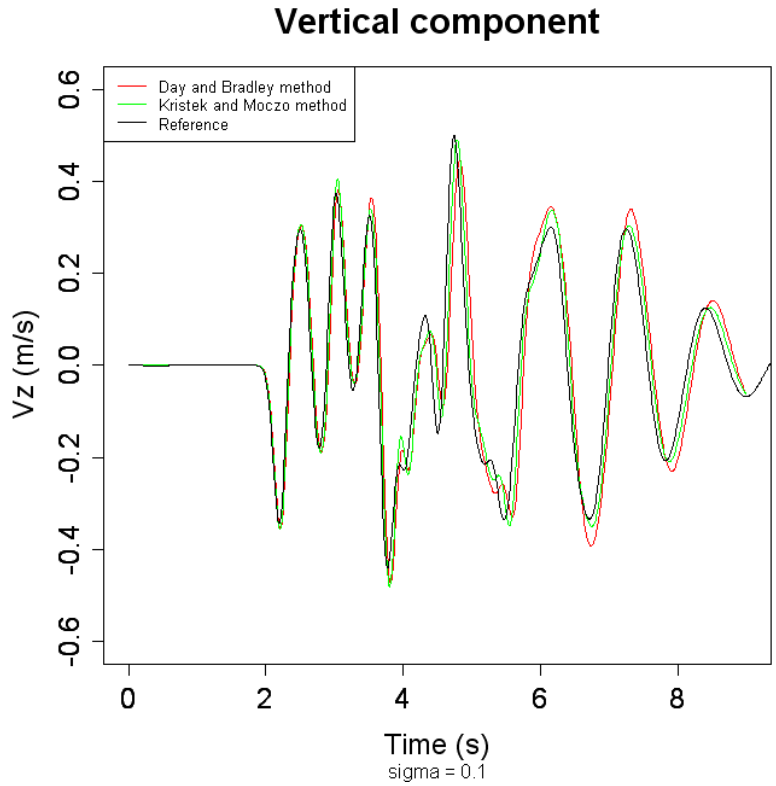

Figure 24 ï Vertical component of the velocity vector for ***ůů*** *= 0.1 for the method of Day and Bradley (red), for the method of Kristek and Moczo (green) and for the reference solution (black).*

For the low frequency filter, there is much less noise than in the case of the high frequency filter. The results of the two methods are compared visually (i.e. no quantitative method of comparison is used). The method of Kristek and Moczo gives more accurate results than the method of Day and Bradley, especially for the transverse component.

Figures 25 to 27 show the results of the simulations for ů = 0.3 for radial, transverse and vertical components of the velocity vector for the two anelasticity methods.

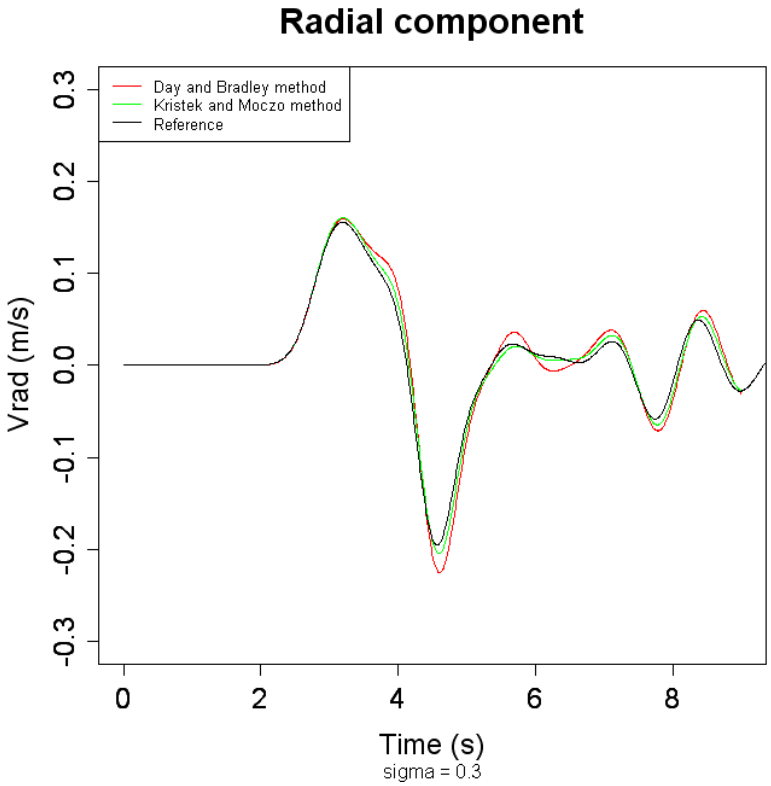

Figure 25 ï Radial component of the velocity vector for $\mathring{u} = 0.3$ *for the method of Day and Bradley (red), for the method of Kristek and Moczo (green) and for the reference solution (black).*

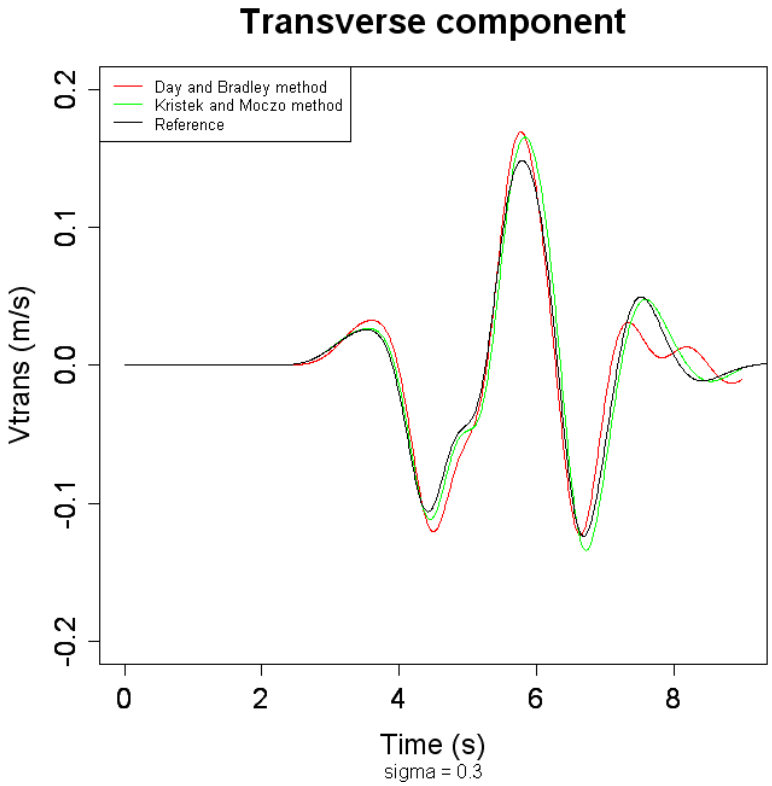

Figure 26 ï Transverse component of the velocity vector for ***ů*** *= 0.3 for the method of Day and Bradley (red), for the method of Kristek and Moczo (green) and for the reference solution (black).*

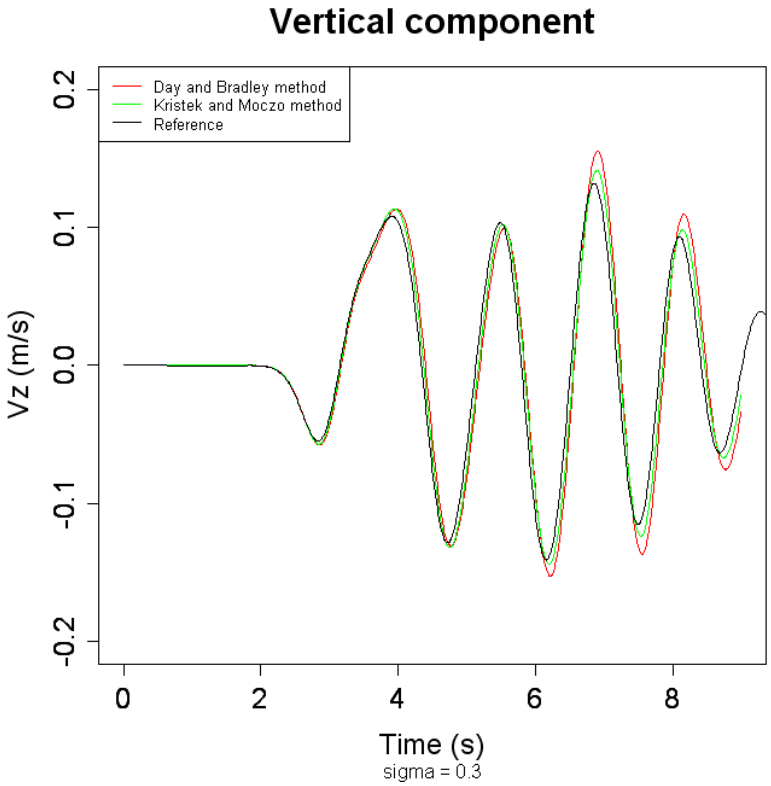

Figure 27 : Vertical component of the velocity vector for $\sigma = 0.3$ for the method of Day and Bradley (red), for the method of Kristek and Moczo (green) and for the reference solution (black).

The very low frequency filter gives results similar to the case of the low frequency filter. There is much less noise than in the case of the high frequency filter and the method of Kristek and Moczo gives more accurate results than the method of Day and Bradley.

The method of Kristek and Moczo is more efficient than the method of Day and Bradley to model the attenuation for the low frequencies. However, as soon as the frequency becomes too high compared to the band of frequency where the anelastic quality factor has been approximated, the simulated seismograms become very noisy and the method of Kristek and Moczo is much less good than the method of Day and Bradley. The latter method allows modelling the quality factor on a larger band of frequency, but with less accuracy.

3.4. CASE OF AN EXTREMELY ANELASTIC LAYER

The aim of the fourth series of simulations is to test the efficiency of the two methods when using an extremely anelastic layer.

The model setting is similar to the one used in Kristek and Moczo (2003). There are CPML boundaries on five sides of the model, at x = -7.5 km and x = 7.5 km, at y = -7.5

km and y = 7.5 km, at z = -7.5 km and a free surface at z = 0. The (x, y, z)-Cartesian coordinates are taken as (east, north, upward). The size of the grid cell is qpx = qpy = qpz = 50 m.

The time step is 0.004 s and the simulation is performed for 2670 time steps.

The source is located at x_{source} = 0 km, y_{source} = 0 km, z_{source} = - 525 m.

The moment rate function m(t) of the dislocation source is a Gabor signal given in Equation (54).

$$m(t) = M_0 \exp\left(-\left(\frac{\varpi\left(t - t_S\right)}{\gamma}\right)^2\right)\cos\left(\varpi\left(t - t_S\right) + \theta\right) \qquad \textbf{(54)}$$

The parameters of the moment rate function are $M_0 = 10^{16}$ N.m, ɔ = 1.5, ϒ = 2´ f_p, f_p = 0.225, ɗ = ´ /2 and t_s = 3.

The parameters of the source are strike ű = 0, dip ŭ = ´ /4 and rake ə = ´ /2.

There are two layers of material. The width of the top layer is 200 m. The corresponding anelasticity parameters are Q_{S0} = 5, Q_{P0} = 10. P- and S-wave velocities and density are respectively V_P = 1125 m.s^{-1}, V_S = 625 m.s^{-1} and ɟ = 1600 kg.m^{-3}.

The anelasticity parameters of the second layer are Q_{S0} = 50, Q_{P0} = 100. P- and S-wave velocities and density are respectively V_P = 5468 m.s^{-1}, V_S = 3126 m.s^{-1} and ɟ = 1800 kg.m^{-3}.

There are 20 receivers located at $x_{receiver}$ = 0, $y_{receiver}$ = 1475 + (n-1) * 400 m, $z_{receiver}$ = -25 m, with n = 1, é , 20.

The anelasticity parameters for the method of Kristek and Moczo are chosen as in Kristek and Moczo (2003) paper: ω_{min} = 2´ *10$^{-7/4}$ and ω_{max} = 2´ *10$^{-1/4}$. The parameters for the method of Day and Bradley are Ǘ$_m$ = 0.1*2´ /ω_{max} and Ǘ$_M$ = 10*2´ /ω_{min}.

The results of the simulations are then compared with the results obtained with the discrete-wavenumber code AXITRA (Coutant, 1989; Bouchon, 1981).

Figures 28 to 30 show seismograms of the simulations for each component of the velocity vector for the two anelastic methods at receiver 1.

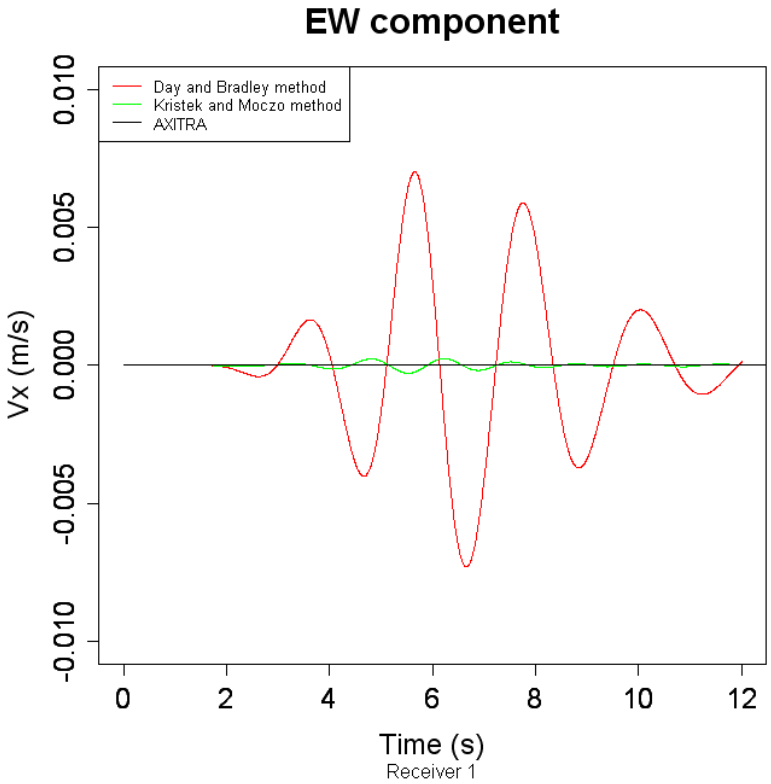

Figure 28 ï EW component of the velocity vector for the method of Day and Bradley (red), the method of Kristek and Moczo (green) and the AXITRA code (black) at receiver 1.

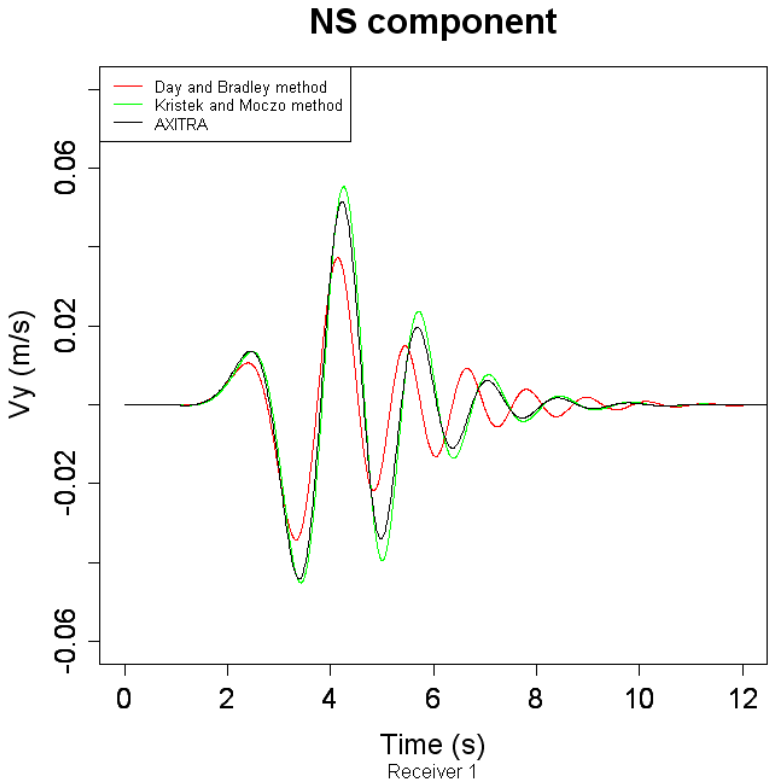

Figure 29 ï NS component of the velocity vector for the method of Day and Bradley (red), the method of Kristek and Moczo (green) and for AXITRA code (black) at receiver 1.

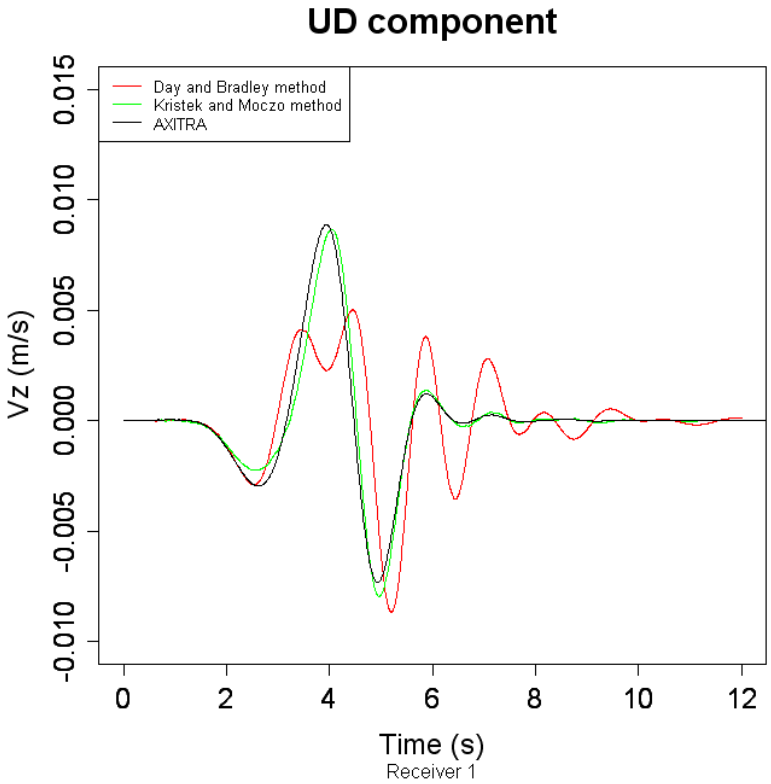

Figure 30 : UD component of the velocity vector for the method of Day and Bradley (red), the method of Kristek and Moczo (green) and the AXITRA code (black) at receiver 1.

For the receiver 1, which is near from the source, there is a good agreement between the results with the method of Kristek and Moczo and the reference result with the AXITRA code. The method of Day and Bradley is much less accurate and attenuate too much the signal. Indeed, as shown in Day (1998), this method is not very accurate for very low anelastic quality factors and, for instance, when we want to impose a quality factor Q equal to 20, the method gives results nearer from a value of Q of 19.

Figures 31 to 33 show seismograms of the simulations for each component of the velocity vector for the two anelastic methods at receiver 10.

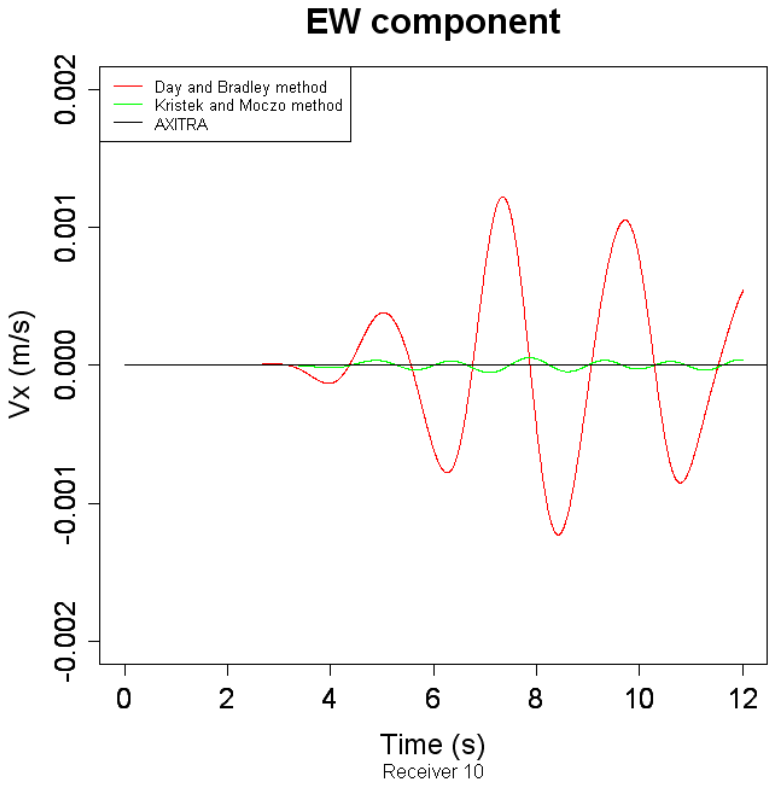

Figure 31 ï EW component of the velocity vector for the method of Day and Bradley (red), the method of Kristek and Moczo (green) and the AXITRA code (black) at receiver 10.

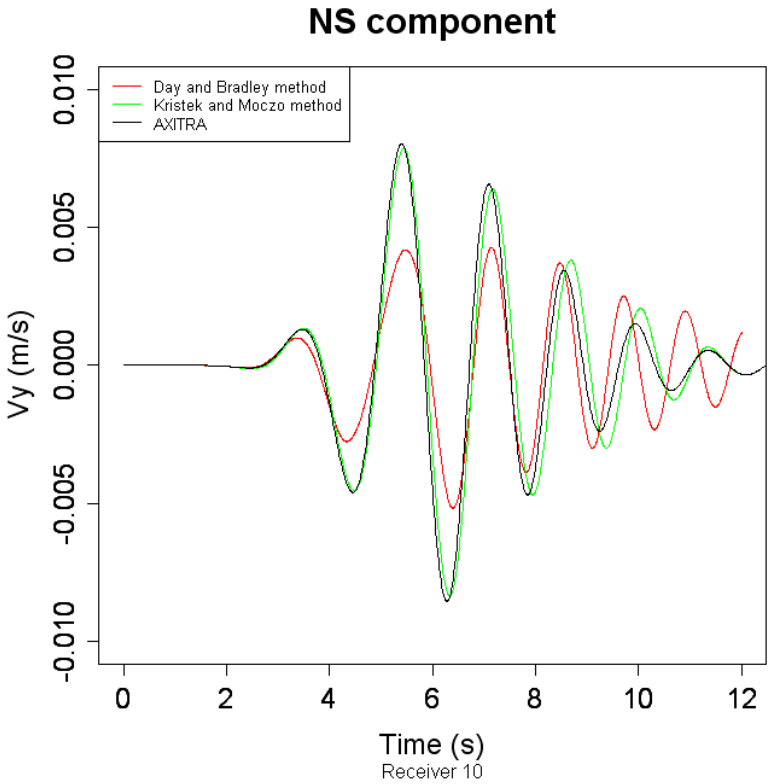

Figure 32 : NS component of the velocity vector for the method of Day and Bradley (red), the method of Kristek and Moczo (green) and for AXITRA code (black) at receiver 10.

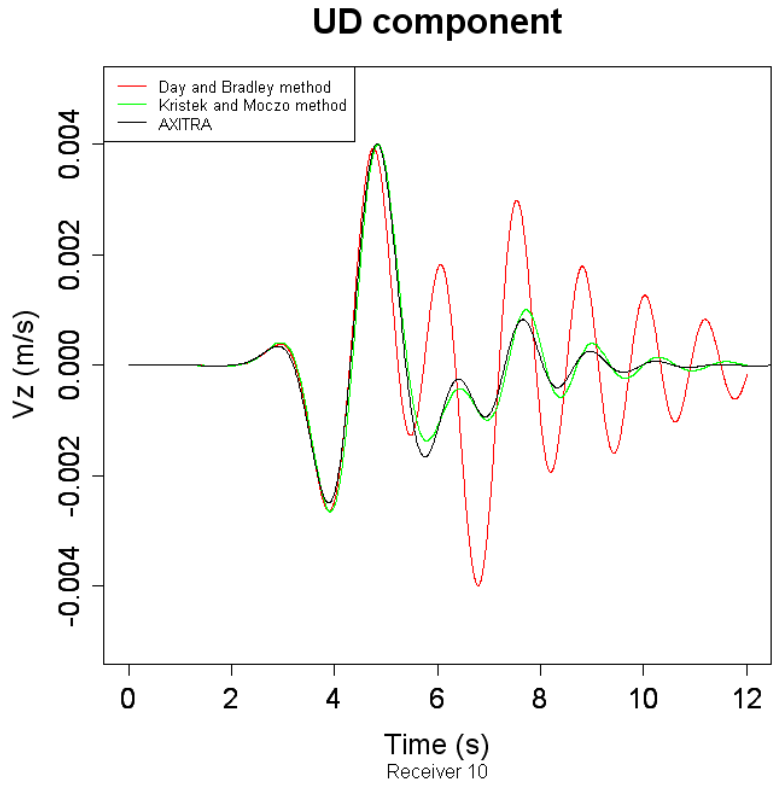

Figure 33 ï UD component of the velocity vector for the method of Day and Bradley (red), the method of Kristek and Moczo (green) and the AXITRA code (black) at receiver 10.

For the receiver 10, which is farther from the source, the agreement between the results with the method of Kristek and Moczo and the reference result remains good. The method of Day and Bradley is much less accurate and attenuate too much the signal.

4. Conclusion

The implementation in the finite differences code ONDES3D of the anelastic methods of Day and Bradley (2001) and Kristek and Moczo (2003) has been explained. The efficiency of the two methods was tested and the results of both methods were compared.

In the general case, the method of Kristek and Moczo is more efficient than the method of Day and Bradley. It can model more accurately very anelastic layers and low frequency signals. However, the method of Kristek and Moczo is less accurate for high frequency signals and the CPML is less efficient with this method.

5. References

Bouchon, M. (1981) ï A simple method to calculate Greenôs functions for elastic layered media. *Bull. Seism. Soc. Am.*, **71**, 959-971.

Collino, F., Tsogka, C. (2001) - Application of the PML absorbing layer model to the linear elastodynamic problem in anisotropic heterogeneous media. *Geophysics*, **66**(1), 294-307.

Coutant, O. (1989) - Program of numerical simulation AXITRA. Res. Rep. LGIT, Université Joseph Fourier, Grenoble (in French).

Day, S.M. (1998) - Efficient Simulation of Constant Q Using Coarse-Grained Memory Variables. *Bull. Seism. Soc. Am.*, **88**, 1051-1062.

Day, S.M., Bradley, C.R. (2001) - Memory-Efficient Simulation of Anelastic Wave Propagation. *Bull. Seism. Soc. Am.*, **91**, 529-531.

Day, S.M., Bielak, J., Dreger, D., Larsen, S., Graves, R., Pitarka, A., Olsen, K.B. (2003) ï Final report to Pacific Earthquake Engineering Research Center ï Lifelines program task 1A02 ï Tests of 3D elastodynamic codes.

Graves, R.W. (1996) - Simulating Seismic Wave propagation in 3D Elastic Media Using Staggered-Grid Finite Differences. *Bull. Seism. Soc. Am.*, **86**, 1091-1106.

Komatitsch, D., Martin, R. (2007) - An unsplit convolutional Perfectly Matched Layer improved at grazing incidence for the seismic wave equation. *Geophysics*, **72** (5), SM155-SM167.

Kristek, J., Moczo, P. (2003) - Seismic-Wave Propagation in Viscoelastic Media with Material Discontinuities: A 3D Fourth-Order Staggered-Grid Finite-Difference Modeling. *Bull. Seism. Soc. Am.*, **93**, 2273-2280.

Lee-tin-yien, Y. (2009) ï Propagation dôondes sismiques en milieu complexe. Rapport de stage de fin dœtudes (in French).

Madariaga, R. (1976) - Dynamics of an expanding circular fault. *Bull. Seism. Soc. Am.*, **65**, 163-182.

Moczo, P., Kristek, J., Vavryļuk, V., Archuleta, R.J., Halada, L. (2002) - 3D Heterogeneous Staggered-Grid Finite-Difference Modeling of Seismic Motion with Volume Harmonic and Arithmetic Averaging of Elastic Moduli and Densities. *Bull. Seism. Soc. Am.*, **92**, 3042-3066.

Nowick, A.S., Berry, B.S. (1972) - *Anelastic relaxation in Crystalline Solids*. Academic Press, New York.

Virieux, J. (1986) - P-SV wave propagation in heterogeneous media: velocity-stress finite-difference method. *Geophysics*, **51**, 889-901.

Scientific and Technical Centre
Natural Risks and CO_2 Storage Security Division
3, avenue Claude-Guillemin - BP 6009
45060 Orléans Cedex 2 ï France ï Tel.: +33 (0)2 38 64 34 34